Journal of Asian Earth Sciences 210 (2021) 104687

Contents lists available at ScienceDirect

Journal of Asian Earth Sciences

journal homepage: www.elsevier.com/locate/jseaes

Early–Middle Jurassic magmatic rocks along the coastal region of southeastern China: Petrogenesis and implications for Paleo-Pacific plate subduction

Jiao-Long Zhao [a,b,*], Jian-Sheng Qiu [b], Liang Liu [c]

[a] School of Earth Sciences, Key Laboratory of Mineral Resources in Western China (Gansu Province), Lanzhou University, Lanzhou 730000, China
[b] State Key Laboratory for Mineral Deposits Research, School of Earth Sciences and Engineering, Nanjing University, Nanjing 210023, China
[c] State Key Laboratory of Ore Deposit Geochemistry, Institute of Geochemistry, Chinese Academy of Sciences, Guiyang 550081, China

ARTICLE INFO

Keywords:
Early–Middle Jurassic granitoids
Petrogenesis
Juvenile crust
Southeast coast of China

ABSTRACT

This study presents new zircon U–Pb ages and whole-rock geochemical data for the Fanyindong (FYD) and Jincheng (JC) granitoid intrusions in coastal Zhejiang and Fujian Provinces, respectively, southeast China, to investigate their petrogenesis and provide new constraints on the regional tectonic evolution and crustal growth. Zircon U–Pb ages indicate that the FYD and JC intrusions were emplaced at c. 170 Ma and 193 Ma, respectively. Both granitoids belong to the high-K calc-alkaline series, and display arc-like trace element patterns, with enrichment of large ion lithophile elements and Nb-Ta depletion. The FYD granitoids show adakitic geochemical characteristics, with high radiogenic Sr isotope ratios, and the most enriched bulk-rock Nd and zircon Hf isotopic compositions (crustal Nd–Hf model ages = ca. 2.35–2.75 Ga) ever reported in the Mesozoic granitoids within southeast China. Geochemical characteristics suggest that the FYD granitoids were generated by partial melting of mostly Paleoproterozoic basement rocks in a thickened lower crust. However, whole-rock Sr–Nd and zircon Hf isotopes of the JC granites show depleted source signatures. Geochemical signatures suggest the JC granites originated from the partial melting of a mixed source, consisting of the pre-existing, ancient, lower crust and juvenile, mantle-derived, basaltic rocks. The data from this study, in conjunction with previously published data, indicates that there exists a NE-trending, Early–Middle Jurassic, arc-related, magmatic rock belt along the southeast coast of China, and the Paleo-Pacific Plate subduction most likely started at c. 200 Ma. The early stage subduction of the Paleo-Pacific plate and the induced reactivation and extension of pre-existing E–W striking faults in the Nanling region of southeastern China gave rise to the generation of the JC granites. Ongoing subduction of the Paleo-Pacific plate resulted in a thickening of the continental margin, and subsequent crustal anatexis of basement materials produced the FYD granitoids.

1. Introduction

The Mesozoic geology of southeastern China is characterized by widespread granitoids and their volcanic equivalents, as well as minor mafic rocks (Jiang et al., 2015; Li et al., 2014b; Liu et al., 2020; Wang et al., 2020; Zhou et al., 2006). The Triassic and Jurassic igneous rocks are mainly concentrated in the interior of southeastern China, whereas the Cretaceous igneous rocks mainly occur in the coastal region (Fig. 1, Zhou et al., 2006; Liu et al., 2012). The origin and tectonic implications of the Mesozoic magmatic rocks within SE China have been extensively studied, but the geodynamic controls for their generation remain highly controversial (Li and Li, 2007; Liu et al., 2020; Zhou et al., 2006; Zhou et al., 2018). Previous studies suggest that Mesozoic tectono-magmatic activities were controlled by both the earlier Tethys orogenic regime and the later Paleo-Pacific regime. The change in the regional tectonic regime took place during the Early Jurassic, which corresponds to a magmatic quiescence stage lasting from 205 Ma to 180 Ma (He et al., 2010; Zhou et al., 2006). Later studies, such as Li and Li (2007) and Li et al. (2012a), advocated that initial subduction of the Paleo-Pacific Plate took place during the Late Permian, and proposed a model with flat-slab subduction followed by slab-foundering, to account for both the Indosinian orogeny and the broad spatial distribution of the Late

* Corresponding author at: School of Earth Sciences, Key Laboratory of Mineral Resources in Western China (Gansu Province), Lanzhou University, Lanzhou 730000, China.
E-mail address: jlz@lzu.edu.cn (J.-L. Zhao).

https://doi.org/10.1016/j.jseaes.2021.104687
Received 22 September 2020; Received in revised form 25 October 2020; Accepted 19 January 2021
Available online 3 February 2021

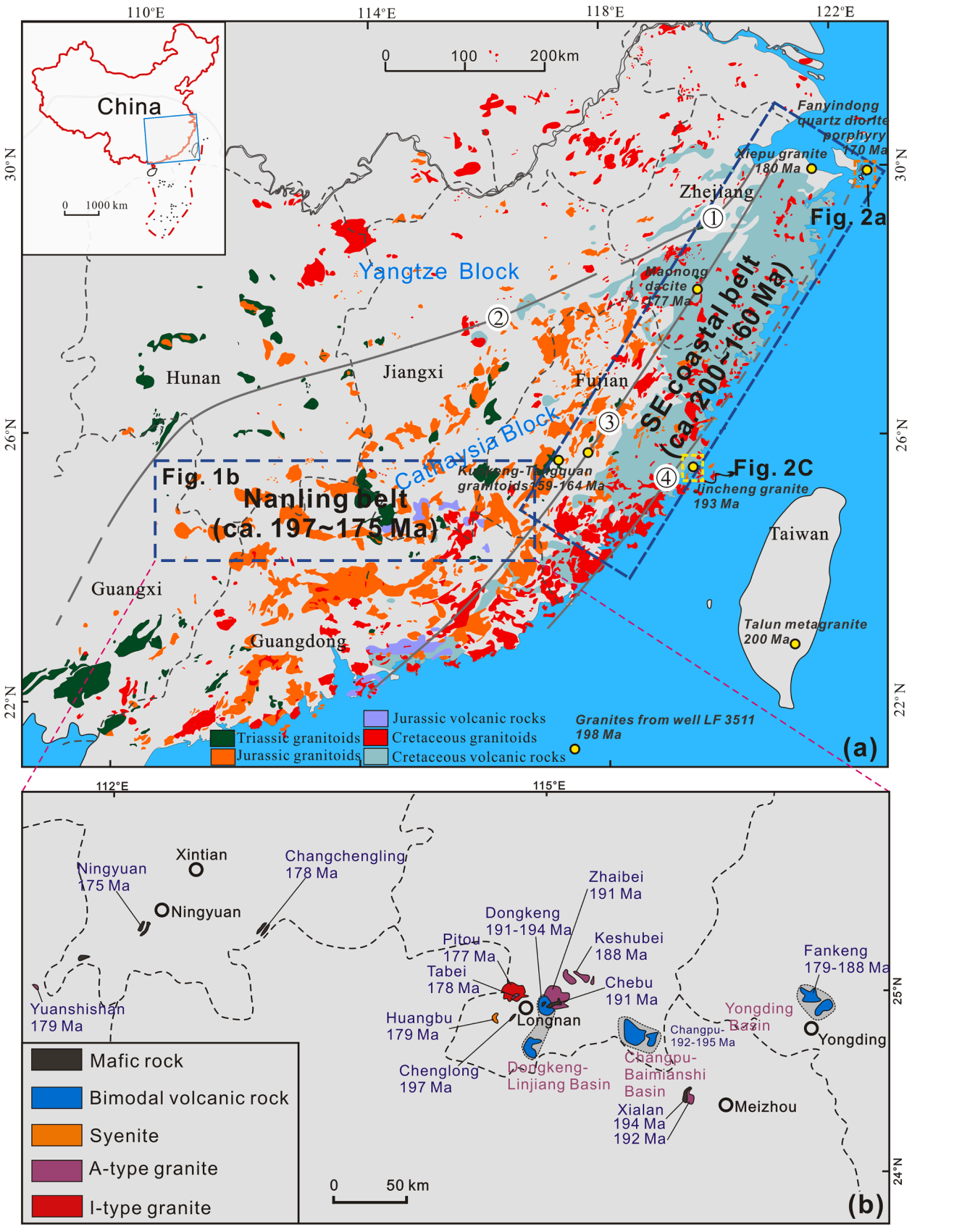

(caption on next page)

Fig. 1. (a) Simplified geological map of southern China showing the distribution of Mesozoic granitoid and volcanic rocks (modified after Zhou et al., 2006), (b) Distribution of the Early Jurassic igneous rocks in the Nanling Range, Southeast China (modified from Bai et al., 2015, Cen et al., 2016). Data sources: Xialan gabbro and granite from Zhu et al. (2010); Changchengling basalt, Chebu and Chenglong gabbro and Keshubei granite from Jiang et al. (2015); Tabei and Huangbu syenite and Pitou granite from He et al.(2010); Zhaibei granite from Jiang et al. (2017); Dongkeng, Changpu and Yongding bimodal volcanic rocks fromCen et al. (2016) and references therein. Yuanshishan granite from Zhou et al. (2018); Ningyuan basalt from Li et al. (2004); Talun granite from Yui et al. (2017);Tangquan-Kuokeng granitoids from Wang et al. (2015) and Li et al. (2016a); Xiepu granite from Li et al. (2012c); Maonong dacite from Liu et al. (2012); Granites of well LF3511 from Xu et al. (2017). Names of the fault zones: ①Jiangshan-Shaoxing fault; ②Pingxiang-Yushan fault; ③Zhenghe-Dapu & Lishui-Yuyao fault; ④Changle–Nan'ao fault. The Early-Middle Jurassic, nearly E–W-striking, magmatic rock belt within Nanling region is abbreviated as Nanling belt; the NE-trending, Early–Middle Jurassic, arc-related, magmatic rock belt along the southeast coast of China is abbreviated as SE coastal belt.

Mesozoic magmatic province. Based on studies of the Jurassic granites, basic rocks, and bimodal volcanic rock associations (ca. 180–154 Ma) within the Nanling region of south China, Chen et al. (2002, 2008) proposed that these rocks are the products of post-collisional extension of the Indosinian orogeny related to the large-scale Tethyan tectonics at this time, marking then the beginning of the Paleo-Pacific system. The sporadically exposed Early-Middle Jurassic magmatic rocks within the coastal areas of southeast China (Fig. 1, Li et al., 2012a; Xu et al., 2017; Zhou et al., 2018) are thought to be the closest magmatic rocks to the convergent plate boundary between the South China Block and the Paleo-Pacific plate. These rocks thus not only offer new insights into the temporal-spatial distribution of Mesozoic magmatic activity in southeast China, but also provide an excellent target to constrain the timing of the Mesozoic tectonic transition from the Tethys orogenic regime to the Paleo-Pacific regime.

Increasingly, studies of the isotopic and geochemical characteristics of Cretaceous and Late Jurassic granitoids in the coastal regions of southeast China have suggested the involvement of partial mantle melts due to the depleted Sr–Nd–Hf isotopic signatures they exhibit (Li et al., 2014b; Yang et al., 2018; Zhao et al., 2016). It is generally accepted that the Late Mesozoic granitoids in the coastal areas of southeast China were mainly generated by mixing of depleted, mantle-derived, mafic magmas with ancient, crustal-derived, felsic magmas (Liu et al., 2013; Zhao et al., 2016). However, recent studies propose that partial melting of the newly formed lower crust associated with the underplated mafic magmas is a first-order control on the formation of the Late Mesozoic granitoids with relatively depleted isotopic characteristics (Chen et al., 2017; Li et al., 2012b; Li et al., 2020; Zhou et al., 2018). The source(s) and petrogenesis of these rocks thus remain to be clarified. In particular, discerning the nature of the ancient basement materials in the coastal region of southeast China is vital for understanding the origins of these granitic rocks and placing constraints on the evolution of the crust in this area. However, finding and studying these rocks is complicated due to the near-complete coverage of the ancient basement rocks in this area by Mesozoic volcanic-sedimentary rocks (Xu et al., 2007). Furthermore, these rocks are often strongly reworked by Mesozoic magmatism with significant input of mantle-derived juvenile materials (Liu et al., 2012; Xu et al., 2007).

This study identifies an Early Jurassic, source-depleted, I-type granite (the Jincheng pluton) in the coastal Fujian Province and a Middle Jurassic, I-type granitoid (the Fanyindong pluton) in the coastal Zhejiang Province, with geochemical characteristics that suggests derivation by reworking of ancient crustal materials. Further, an Early–Middle Jurassic arc-related magmatic rock belt is recognized along the southeast coast of China (Fig. 1, SE coastal belt). These discoveries are thus significant toward further understanding the Late Mesozoic

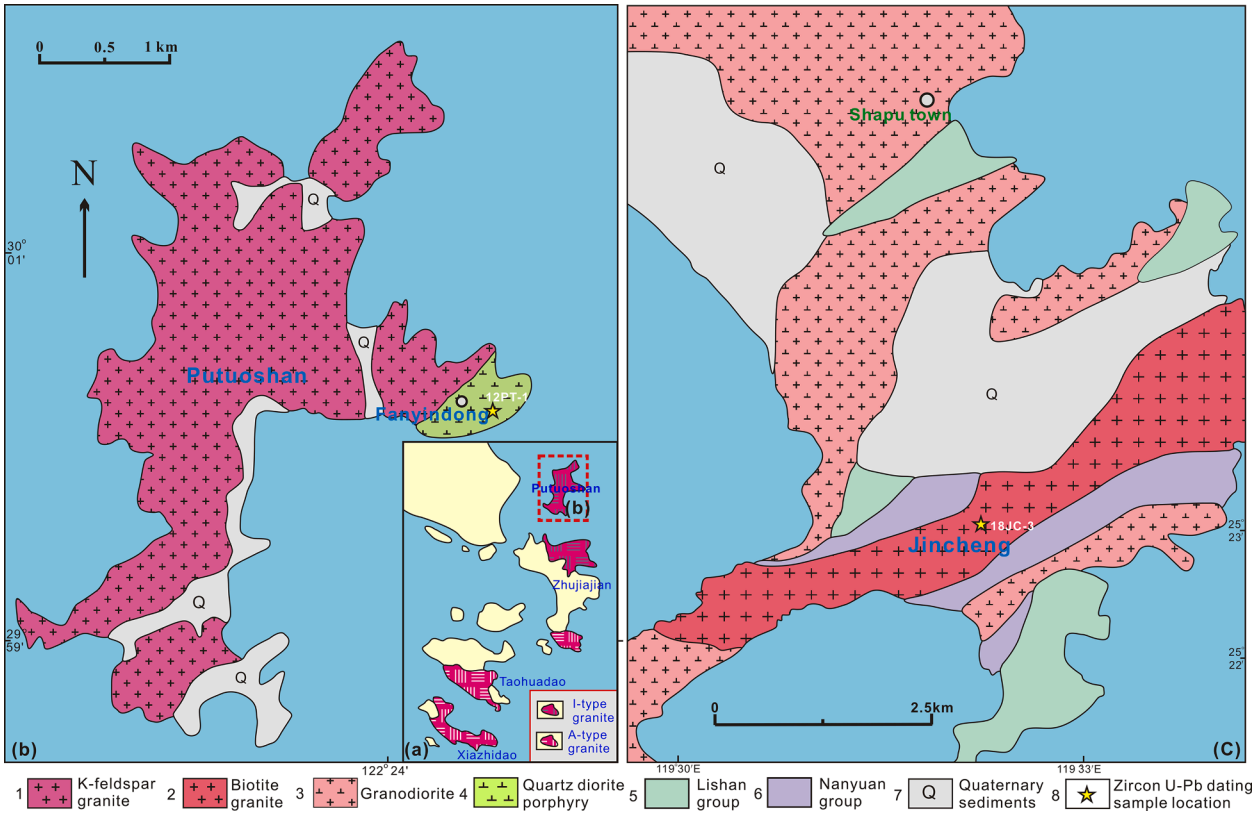

Fig. 2. (a) Simplified geological map of the Zhoushan archipelago, showing the location of Putuoshan Island. (b) Simplified geological map of the Fanyindong intrusion in the Putuoshan Island (modified after Zhao et al., 2016); (c) Simplified geological map of the Jincheng pluton (modified after Liu et al., 2011).

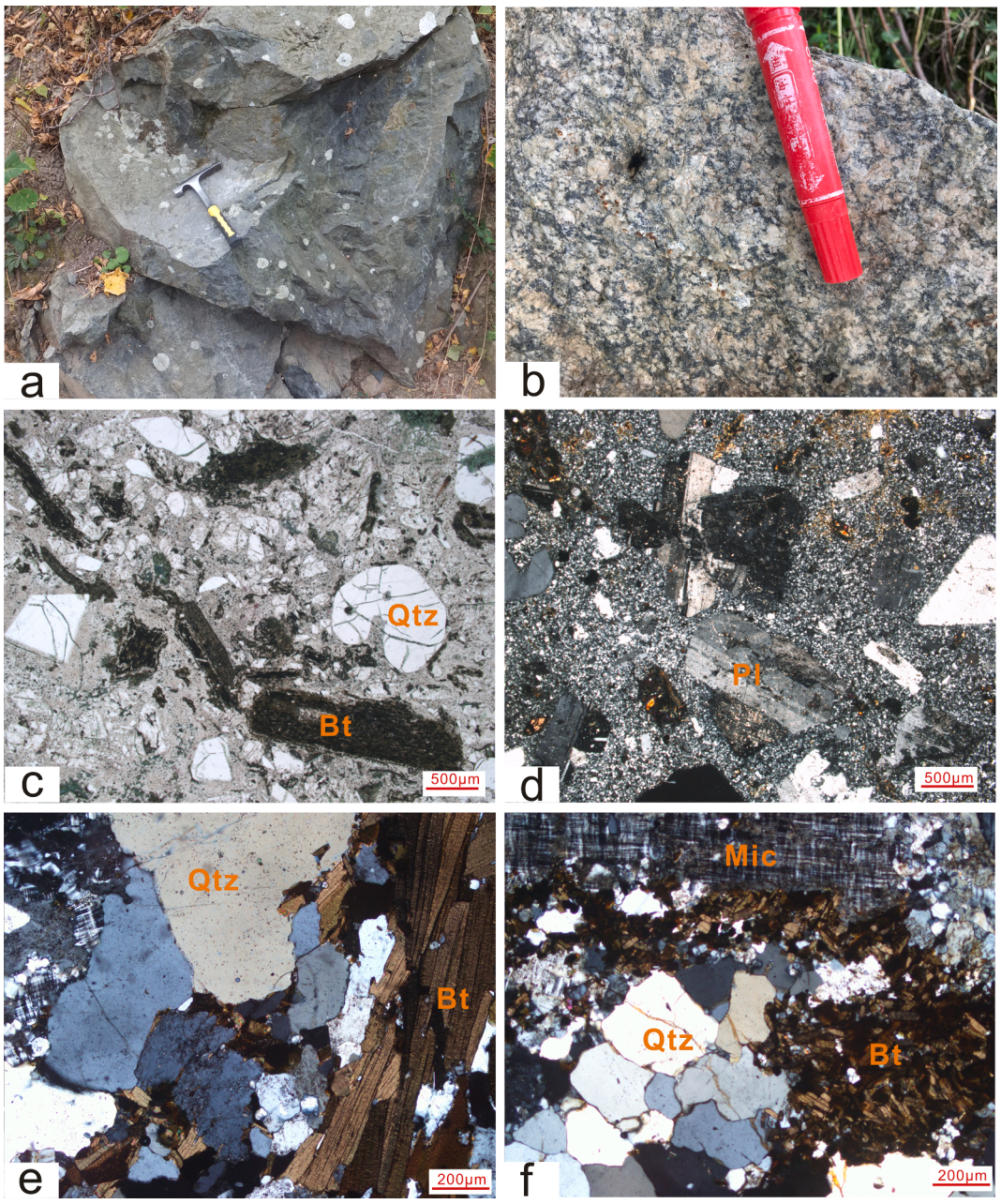

Fig. 3. (a), (c) and (d) Macroscopic photos and photomicrographs of quartz diorite porphyry from the Fanyindong pluton; (b), (e) and (f) macroscopic photos and photomicrographs of granites from the Jincheng pluton. Mineral abbreviation: Qtz–quartz; Mic– microcline; Pl– plagioclase; Bt– biotite. The photomicrographs (c) was taken using plane-polarized light, and all other thin section photos were taken under cross-polarized light.

geology of southeast China. Herein, we present the zircon U–Pb ages, major- and trace-element concentrations, and Sr–Nd–Hf isotopic compositional data for the Fanyindong (FYD) and Jincheng (JC) granitoids, to elucidate the granitoid source compositions and place new constraints on the Mesozoic growth of the South China Crust and the geodynamic setting of the magmatism.

2. Geological background

The South China Block is located on the eastern margin of Eurasia. It consists of the Yangtze Block in the northwest and the Cathysia Block in the southeast, which were amalgamated during the Neoproterozoic (Li et al., 2009; Wang et al., 2006; Zheng et al., 2007). The Jiangshan–-Shaoxing Fault Zone is generally regarded as the boundary between these two blocks in southeastern China, but poor exposure and thermo-tectonic reworking obfuscate the southwestern extension of this boundary. The Cathaysia Block experienced extensive and widespread polyphase orogenesis and magmatism during the Phanerozoic, and is widely covered by Phanerozoic sedimentary and volcanic rocks, with only sporadically exposed Precambrian basement rocks (Li et al., 2014a; Xu et al., 2007; Yu et al., 2010). These basement rocks are mainly distributed to the west of the Zhenghe–Dapu fault, including the c. 1.8 Ga Badu complex in the southwestern Zhejiang Province, the c. 0.8 Ga Chencai complex in the northwestern Zhejiang Province, and the ~0.8–0.7 Ga Mamianshan and Mayuan Groups in the western Fujian Province (Li et al., 2014a; Yu et al., 2010; Wang et al., 2018).

Late Mesozoic magmatism was largely confined to the Cathaysia Block and eastern Yangtze Block, with magmatic activity increasing from the geographic interior toward the coast (Liu et al., 2020; Zhou et al., 2006). Jurassic magmatic rocks are mainly distributed in the

interior of the Cathaysia Block, preferentially along a NE–SW-trending direction (Li et al., 2020; Liu et al., 2020; Zhou et al., 2006). They are dominated by calc-alkaline I-type granites, subordinate syenites, and A- and S-type granites, mainly formed during a short time interval between 165 Ma and 155 Ma (Liu et al., 2020; Zhou et al., 2006). Except in the case of the Nanling region, the Early-Middle Jurassic rocks (190–170 Ma), such as syenites, A-type granites, bimodal volcanic-, and intrusive rock associations constitute an E–W strike magmatic belt (namely, Nanling belt) exceeding 500 km long (Fig. 1, He et al., 2010; Liu et al., 2011; Zhou et al., 2018). There are also some ca. 167–172 Ma porphyries in northeastern Jiangxi and northwestern Zhejiang provinces, which are associated with Cu–Au mineralization (Wang et al., 2012). In contrast, the Cretaceous magmatic rocks are primarily concentrated in the coastal Fujian and Zhejiang Provinces (Li et al., 2014b; Liu et al., 2020; Yang et al., 2018; Zhao et al., 2016). The Cretaceous intrusive rocks of southeast China are dominantly high-K calc-alkaline, I-type granites with lesser A-type granites and basic rocks. These type of rocks generally have close spatial relationships, demonstrated by characteristic I- and A-type composite granitic plutons and gabbro–granite complexes (Li et al., 2014b; Zhao et al., 2016).

3. Petrography

The FYD quartz diorite porphyry, with an outcrop area of ~0.48 km^2, is located in the Zhoushan archipelago within the coastal area of the Zhejiang Province, and is intruded by the dominant I-type, K-feldspar granites and peralkaline A-type granites (Fig. 2). The FYD pluton ranges in colors from grey to dark grey (Fig. 3a), and shows a porphyroclastic texture that is characteristic of subvolcanic rocks (Fig. 3c and d). The phenocrysts (ca. 10–15 vol%) are predominantly composed of quartz and plagioclase with minor amphibole and biotite, and show various degrees of fragmentation (i.e., cataclastic texture). The quartz grains are rounded and embayed (Fig. 3c) indicating partial resorption prior to emplacement. The groundmass displays a microcrystalline texture, and consists mainly of fine-grained quartz, plagioclase and amphibole, with minor opaque oxides, apatite, allanite, and zircon. Both the amphibole and biotite phenocrysts are almost fully altered to chlorite and sericite, with precipitation of Fe-oxides (Fig. 3c and d). Plagioclase crystals (An % = 31–36) occur as subhedral laths with Carlsbad-albite twinning.

The JC biotite granites are located in the Shapu region of Fuqing City, Fujian Province, and are unconformably overlain by the Late Jurassic Lishan Formation and Early Cretaceous Nanyuan Formation (Fig. 2c). The JC biotite granites have well-developed tectonic foliation defined by biotite alignment as a result of metamorphic overprinting (Fig. 3b). The granites are gray in color and have equigranular–porphyritic textures. The phenocrysts (ca. 10–15 vol%) are mainly composed of K-feldspar (5–8 mm in size) and quartz (4–6 mm in size) (Fig. 3e and f). The groundmass is fine- to medium-grained, and is composed of quartz, biotite, K-feldspar, and plagioclase, with accessory zircon and magnetite. Perthite is locally abundant and occasionally displays Carlsbad twins, while microcline is more common both in phenocrysts and the groundmass (Fig. 3e and f). The biotite grains are dark reddish-brown in color and occasionally show strong deformation.

4. Sampling and analytical methods

4.1. Zircon U–Pb dating and Hf isotopes

Zircons from the FYD quartz diorite porphyry (sample 12PT-1, GPS position: N30°00′10.0′′, E122°24′38.0′′) and the Jincheng biotite granite (sample 18JC-3, GPS position: N25°23′4.63′′ E119°32′16.8′′) were separated by conventional techniques, including crushing, sieving, and magnetic and heavy liquid separation methods. Zircon grains, handpicked under a binocular stereomicroscope, were mounted in epoxy resin, and polished to expose their centres. The external morphology and internal structure of grains were characterized using transmitted and reflected light microscopy and cathodoluminescence (CL) images to guide the selection of analytical spots. The CL images were obtained using a Mono CL3+ (Gatan, Pleasanton, CA, USA) attached to a scanning electron microscope (Quanta 400 FEG, Hillsboro, OR, USA) at the State Key Laboratory of Continental Dynamics, Northwest University, Xi'an, China.

Zircon U–Pb isotopic analyses were carried out using an Agilent 7500a inductively coupled plasma–mass spectrometer (ICP–MS) coupled to a New Wave Research 213-nm laser ablation system at the State Key Laboratory for Mineral Deposits Research (SKLMDR), Nanjing University. The ablated material was transported in a He carrier gas through PVC tubing (inner diameter, 3 mm) and combined with argon in a 30 cm^3 mixing chamber prior to entry into the mass spectrometer. Analyses were carried out using a beam diameter of 25 μm, repetition rate of 5 Hz, and energy of 23.74–26.68 J/cm^2. Date acquisition for each analysis took 100 s (40 s on background signal, 60 s on ablated signal). A homogeneous standard zircon (GEMOC GJ-1: $^{207}Pb/^{206}Pb$ age of 608.5 ± 0.4 Ma and a relatively young $^{206}Pb/^{238}U$ age of 599.8 ± 4.5 Ma, Jackson et al., 2004) was used to correct the mass discrimination of the mass spectrometer and residual elemental fractionation. A well-characterized zircon standard (Mud Tank; intercept age, 732 ± 5 Ma; Black and Gulson, 1978) was used as an independent control on reproducibility and instrument stability. The raw ICP–MS U–Pb isotopic data were processed using GLITTER 4.4. Common Pb corrections were performed using the method described by Andersen (2002).

In situ zircon Hf isotope analyses were performed using a Thermo Scientific Neptune Plus multi-collector (MC) ICP–MS attached to a New Wave UP193 solid-state laser ablation system at the SKLMDR, Nanjing University. Zircons were ablated with a beam diameter of 35 μm, energy of 9.54–11.35 J/cm^2, and an 8 Hz laser repetition rate. Two reference standards were also measured to evaluate the reliability of the data (Mud Tank zircon $^{176}Hf/^{177}Hf$ ratio = 0.282501 ± 0.000004, n = 23, 2σ; 91,500 zircon $^{176}Hf/^{177}Hf$ ratio = 0.282316 ± 0.000009, n = 9, 2σ) before analyses of unknown samples. The measured $^{176}Hf/^{177}Hf$ ratios of the two standards agree with the recommended values within 2σ error (Griffin et al., 2006).

4.2. Whole-rock major and trace element, and Sr–Nd isotope analyses

All samples selected for chemical and isotopic analyses were crushed and powdered to 200 mesh using an agate mill for whole-rock geochemical analysis.

Whole-rock major elements, trace elements, and Sr–Nd isotopic compositions of the FYD pluton were determined at the SKLMDR, Nanjing University, China. For major element analyses, mixtures of whole-rock powders (0.5 g) and $Li_2B_4O_7$ + $LiBO_2$ + LiBr (11 g) were made into glass discs and then analysed using a Thermo Scientific ARL 9900 X-ray fluorescence (XRF) spectrometer. The analytical precision was estimated to be less than 10% for all major elements and less than 1% for the majority of elements. For trace element analyses, ~50 mg of powder was dissolved in high-pressure Teflon bombs using a HF + HNO_3 mixture; Rh was used as an internal standard to monitor for signal drift during the ICP–MS analyses. Trace element concentrations were determined using a Finnigan Element II ICP–MS. Detailed analytical procedures followed Gao et al. (2003). The analytical precision was better than 10% for all trace elements, with the majority being better than 5%. For whole-rock Sr–Nd isotope analyses, ~50 mg of powder was dissolved in the same way as for trace element analyses. Rb–Sr and Sm–Nd were separated using AG50W × 8 resin and various eluents. Rare earth elements (REEs) were first separated from Rb–Sr by conventional cation exchange chromatography, using HCl as an eluent. Rb and Sr were then separated and purified using a mixed eluent of pyridinium and DCTA complex. Sm and Nd were separated and purified using HIBA as an eluent, through a small volume of cation exchange resin (0.6 ml). Sr isotopic compositions were measured using a Finnigan Triton TI thermal ionization mass spectrometer, following the methods of Pu et al. (2005).

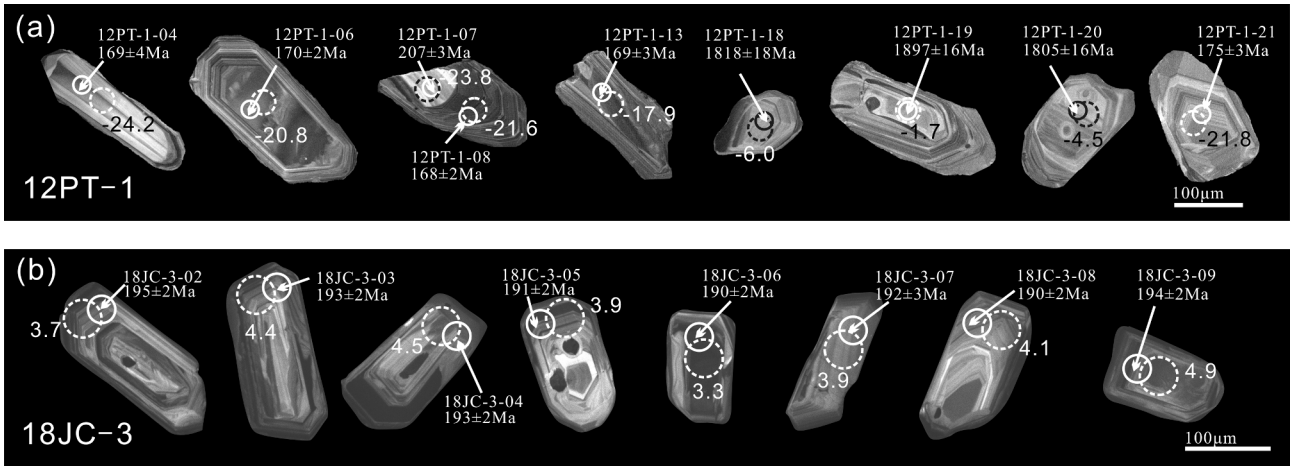

Fig. 4. Representative cathodoluminescence (CL) images of selected zircons from the Fanyindong and the Jincheng plutons. The morphology of zircon grains, $^{206}Pb/^{238}U$ ages, and $\varepsilon_{Hf}(t)$ values are shown. Small solid-line circles represent the U–Pb isotope analyzing positions, and large dashed-line circles represent the analyzing positions for Hf isotopes. The circle diameter is the approximate laser spot size.

Nd isotopic compositions were measured using a Thermo Scientific Neptune Plus multiple-collector ICP–MS. $^{87}Sr/^{86}Sr$ and $^{143}Nd/^{144}Nd$ ratios are reported as measured, after normalization to $^{86}Sr/^{88}Sr = 0.1194$ and $^{146}Nd/^{144}Nd = 0.7219$, respectively, to correct for instrumental fractionation. During the period of this study, measurements of the Japan JNdi-1 Nd standard gave $^{143}Nd/^{144}Nd = 0.512075 \pm 0.000012$ ($n = 11$, 2σ) and the NIST SRM 987 Sr standard yielded $^{87}Sr/^{86}Sr = 0.710248 \pm 0.000004$ (2σ).

Whole-rock major element analyses of the samples from the JC pluton were performed using a PANalytical PW2424 X-ray fluorescence (XRF) spectrometer at the ALS Chemex (Guangzhou) Co. Ltd., China. Mixtures of whole-rock powders (~0.9 g) and lithium borate flux (50%–50% Li_2B4O_7–$LiBO_2$) were fused into glass discs and then analysed by XRF. Loss on ignition (LOI) values were determined by heating 1 g of powder to 1000 °C for 1 h. The analytical precision is generally better than 5%. Trace elements compositions for the samples from JC pluton were measured using an Agilent Technologies 7700x quadrupole ICP–MS (Hachioji, Tokyo, Japan) at Nanjing FocuMS Technology Co. Ltd. About 40 mg powder were mixed with 0.5 ml HNO_3 and 1.0 ml HF in high-pressure PTFE bombs. These bombs were steel-jacketed and placed in the oven for 72 h at 195℃. An internal Rh standard was used to monitor signal drift during counting. The international standards BHVO-2, AGV-2 and GSP-2 were used for monitoring data quality. The analytical precision is estimated to be better than 10%.

Sr and Nd isotope analyses for the JC biotite granites were undertaken using a Thermo Fisher Scientific Neptune Plus MC-ICP-MS at Beijing Createch Testing Technology Co., Ltd. Normalisation to $^{86}Sr/^{88}Sr = 0.1194$ and $^{146}Nd/^{144}Nd = 0.7219$ were employed for mass fractionation corrections. In addition, the Sr isotope international standard NBS-987 was repeatedly tested for accuracy monitoring, yielding an average $^{87}Sr/^{86}Sr$ of 0.710247 ± 17 (n = 13, 2σ). The stability assessment for $^{143}Nd/^{144}Nd$ was conducted with the in-house standard GSB-Nd, yielding $^{143}Nd/^{144}Nd = 0.512179 \pm 18$ (n = 21, 2σ). Detailed analytical procedures are described in Yang et al. (2010).

5. Analytical results

5.1. Zircon U–Pb dating

Cathodoluminescence images of representative zircon grains from the FYD and JC plutons are shown in Fig. 4. The results of the LA–ICP–MS U–Pb isotopic analyses are listed in Table 1 and are presented graphically in Fig. 5.

Zircon grains from the FYD pluton are euhedral prismatic to elongated prismatic in shape, with crystal lengths from 120 to 300 μm and length/width ratios of ca. 1.5:1 to 3.5:1. The zircon crystals are mainly transparent, light yellow to colorless, and exhibit regular magmatic oscillatory zoning in the CL images (Fig. 4). Zircon grains from the JC pluton range from 100 to 200 μm in length, with length/width ratios of 1:1 to 2:1, and have other characteristics similar to 12PT-1. All zircon grains from the FYD and JC plutons have higher Th/U ratios than those of metamorphic zircon (<0.1), supporting the magmatic origin of the zircons (Williams et al., 1996).

A total of 22 analyses were conducted on 18 zircon grains from sample 12PT-1 of the FYD pluton. Eighteen analyses form a near-concordant group, yielding a weighted mean $^{206}Pb/^{238}U$ age of 169.8 ± 1.1 Ma (MSWD = 0.52) (Fig. 5a). According to the CL imaging and experimental records, this is interpreted to represent the crystallization age of the FYD porphyritic intrusion. The remaining four analyses from the zircon cores give older, but contrasting U-Pb ages. One grain has a $^{206}Pb/^{238}U$ age of 207 ± 3 Ma, and the others have $^{207}Pb/^{206}Pb$ ages of 1805–1897 Ma (Table 1, Fig. 5a), possibly representing the ages of inherited zircon cores. Twenty-nine analyses from sample 18JC-3 yield concordant $^{206}Pb/^{238}U$ ages ranging from 189 to 196 Ma. The weighted mean of 192.7 ± 0.9 Ma (MSWD = 1.7) (Fig. 5b) is interpreted as the crystallization age of the JC biotite granite.

5.2. Whole-rock major and trace element characteristics

Representative whole-rock major- and trace-element analyses for the FYD and JC plutons are given in Table 2.

The FYD quartz diorite porphyries are intermediate to slightly felsic in composition (SiO_2 = 63.36–67.04 wt%) and have relatively moderate to high alkali contents ($K_2O + Na_2O$ = 5.97–7.58 wt%), which fall into fields of the granodiorite and subalkaline series on a total alkalis vs. silica (TAS) diagram (Fig. 6a). They have high contents of Al_2O_3 (15.19–16.13 wt%) and CaO (2.95–5.08 wt%), and are metaluminous with A/CNK ratios of 0.92 to 0.97 (Fig. 6c). In contrast, the JC biotite granites have higher SiO_2 (71.15–74.44 wt%), K_2O (4.05–4.77 wt%), total alkalis, and $FeO^T/(FeO^T + MgO)$ ratios, and lower CaO (0.83–1.75 wt%) and MgO (0.37–0.79 wt%) contents. They are weakly peraluminous with A/CNK values of 1.02–1.09. Both plutons can be classified as high-K calc-alkaline series (Fig. 6b). Following the classification of Frost et al. (2001), the JC biotite granites belong to the ferroan subgroup, whereas all samples from the FYD pluton belong to the magnesian subgroup (Fig. 6d).

All of the samples from the FYD and JC plutons are enriched in light rare earth elements (LREE) and large ion lithophile elements (LILE; e.g.,

Table 1
Zircon LA-ICP-MS U-Pb isotopic data of the Fanyindong (FYD) and Jincheng (JC) plutons in southeast coast of China.

Spot no.	Th/U	Isotopic ratios						Ages (Ma)			
		$^{207}Pb/^{206}Pb$		$^{207}Pb/^{235}U$		$^{206}Pb/^{238}U$		$^{207}Pb/^{235}U$		$^{206}Pb/^{238}U$	
		Ratio	±1s	Ratio	±1s	Ratio	±1s	Age	±1s	Age	±1s
12PT-1, coordinate: N30°00′10.0″, E122°24′38.0″											
12PT1-01	0.65	0.04985	0.00099	0.18267	0.00386	0.02658	0.00038	170	3	169	2
12PT1-02	0.45	0.04910	0.00101	0.18007	0.00385	0.02660	0.00037	168	3	169	2
12PT1-03	0.35	0.04998	0.00139	0.18280	0.00510	0.02653	0.00040	170	4	169	3
12PT1-04	2.95	0.04982	0.00311	0.18233	0.01111	0.02657	0.00066	170	10	169	4
12PT1-05	0.32	0.04903	0.00128	0.18156	0.00477	0.02686	0.00039	169	4	171	2
12PT1-06	0.46	0.04895	0.00096	0.18051	0.00374	0.02675	0.00038	168	3	170	2
12PT1-07	1.99	0.05049	0.00200	0.22740	0.00890	0.03267	0.00055	208	7	207	3
12PT1-08	0.40	0.04900	0.00095	0.17847	0.00370	0.02642	0.00038	167	3	168	2
12PT1-09	0.47	0.04976	0.00119	0.18260	0.00437	0.02662	0.00038	170	4	169	2
12PT1-10	0.74	0.04902	0.00128	0.18057	0.00473	0.02672	0.00039	169	4	170	2
12PT1-11	0.48	0.05116	0.00137	0.18689	0.00524	0.02651	0.00046	174	4	169	3
12PT1-12	0.42	0.05232	0.00093	0.19064	0.00370	0.02643	0.00038	177	3	168	2
12PT1-13	0.73	0.04945	0.00154	0.18118	0.00583	0.02658	0.00049	169	5	169	3
12PT1-14	0.43	0.05013	0.00150	0.18223	0.00567	0.02637	0.00048	170	5	168	3
12PT1-15	0.27	0.05169	0.00104	0.19147	0.00416	0.02687	0.00041	178	4	171	3
12PT1-16	0.63	0.05239	0.00180	0.19392	0.00668	0.02685	0.00048	180	6	171	3
12PT1-17	0.63	0.04970	0.00115	0.18653	0.00458	0.02723	0.00044	174	4	173	3
12PT1-18	0.51	0.11111	0.00205	4.90245	0.10249	0.32007	0.00517	1803	18	1790	25
12PT1-19	0.43	0.04970	0.00097	0.18574	0.00384	0.02711	0.00039	173	3	172	2
12PT1-20	1.00	0.11034	0.00183	4.90923	0.09240	0.32271	0.00485	1804	16	1803	24
12PT1-21	0.44	0.04897	0.00118	0.18596	0.00465	0.02754	0.00042	173	4	175	3
12PT1-22	0.70	0.11650	0.00196	5.47692	0.09927	0.34099	0.00470	1897	16	1891	23
18JC-3, N25°23′4.63″ E119°32′16.8″											
18JC-3–01	0.46	0.04865	0.00174	0.20733	0.00603	0.03074	0.00034	191	5	195	2
18JC-3–02	0.45	0.05030	0.00182	0.21314	0.00690	0.03064	0.00034	196	6	195	2
18JC-3–03	0.31	0.04969	0.00184	0.20807	0.00795	0.03040	0.00039	192	7	193	2
18JC-3–04	0.60	0.04840	0.00125	0.20059	0.00539	0.03001	0.00028	186	5	191	2
18JC-3–05	0.47	0.04924	0.00110	0.20312	0.00478	0.02985	0.00027	188	4	190	2
18JC-3–06	0.54	0.05010	0.00202	0.20847	0.00857	0.03015	0.00041	192	7	192	3
18JC-3–07	0.43	0.05144	0.00219	0.21275	0.00764	0.02994	0.00031	196	6	190	2
18JC-3–08	0.52	0.04990	0.00112	0.21102	0.00506	0.03054	0.00028	194	4	194	2
18JC-3–09	0.63	0.05120	0.00175	0.21535	0.00751	0.03049	0.00035	198	6	194	2
18JC-3–10	0.55	0.04850	0.00216	0.19975	0.00732	0.02975	0.00027	185	6	189	2
18JC-3–11	0.28	0.04956	0.00124	0.20346	0.00519	0.02969	0.00029	188	4	189	2
18JC-3–12	0.42	0.04748	0.00153	0.19997	0.00675	0.03043	0.00032	185	6	193	2
18JC-3–13	0.32	0.05057	0.00115	0.21263	0.00487	0.03042	0.00030	196	4	193	2
18JC-3–14	0.59	0.05036	0.00150	0.21543	0.00679	0.03094	0.00038	198	6	196	2
18JC-3–15	0.34	0.04994	0.00145	0.21306	0.00648	0.03092	0.00038	196	5	196	2
18JC-3–16	0.13	0.04857	0.00088	0.20519	0.00391	0.03060	0.00029	190	3	194	2
18JC-3–17	0.52	0.04753	0.00171	0.19806	0.00710	0.03043	0.00031	183	6	193	2
18JC-3–18	0.28	0.04964	0.00122	0.21063	0.00569	0.03081	0.00048	194	5	196	3
18JC-3–19	0.69	0.04911	0.00188	0.20209	0.00771	0.02995	0.00031	187	7	190	2
18JC-3–20	0.72	0.05100	0.00203	0.20993	0.00606	0.02999	0.00030	193	5	191	2
18JC-3–21	0.68	0.04942	0.00171	0.20856	0.00733	0.03056	0.00029	192	6	194	2
18JC-3–22	0.29	0.05251	0.00121	0.22114	0.00524	0.03045	0.00030	203	4	193	2
18JC-3–23	0.66	0.05222	0.00160	0.22263	0.00702	0.03077	0.00034	204	6	195	2
18JC-3–24	0.25	0.05090	0.00132	0.21588	0.00548	0.03072	0.00030	198	5	195	2
18JC-3–25	0.43	0.05114	0.00174	0.21016	0.00594	0.02969	0.00024	194	5	189	2
18JC-3–26	0.14	0.04965	0.00098	0.20976	0.00412	0.03055	0.00032	193	3	194	2
18JC-3–27	0.40	0.04902	0.00169	0.20958	0.00445	0.03081	0.00023	193	4	196	1
18JC-3–28	0.36	0.05054	0.00142	0.21295	0.00575	0.03048	0.00027	196	5	194	2
18JC-3–29	0.81	0.05097	0.00089	0.21669	0.00392	0.03063	0.00027	199	3	195	2

Rb, Cs, and Pb), with variable depletion in Eu, Ba, Sr, P, and Ti (Fig. 7). Despite these commonalities, there is a discordance in trace element abundances between the two plutons. The FYD quartz diorite porphyries are characterized by high Sr (303.5–413.9 ppm), low Y (15.7–20.4 ppm) contents, and high Sr/Y (17.0–25.1) ratios, and show relatively low HREE contents and high La/Yb ratios (23.8–26.2) with significantly fractionated REE patterns (Fig. 7a), suggestive of adakite-like affinity (Defant and Drummond, 1990; Richards et al., 2012). They also have relatively high Zr, Hf, and Ta concentrations. By comparison, the JC biotite granites are relatively depleted in Sr, and enriched in Y and HREEs, with low Sr/Y (0.94–2.29) and La/Yb (5.69–18.4) ratios, and show nearly flat HREE patterns in a chondrite-normalized REE diagram (Fig. 7a). They also have lower Ta, Zr and Hf contents and higher Rb/Sr and Rb/Ba ratios, and more significant depletions in Ti compared with the FYD quartz diorite porphyries (Fig. 7b). Low Ga/Al ratios are observed in both plutons with the occurrence of amphibole, suggestive of I-type granitoids.

5.3. Whole-rock Sr–Nd isotopes

Whole-rock Sr–Nd isotopic compositions of representative samples from the FYD and JC plutons are listed in Table 3 and plotted in Fig. 8. Initial isotopic ratios are calculated using the crystallization age obtained in this study. Both plutons display relatively homogeneous isotopic compositions. Compared with other Mesozoic igneous rocks in southeast China, the FYD quartz diorite porphyries have the highest initial $^{87}Sr/^{86}Sr$ ratios (I_{Sr}, 0.7184 to 0.7211) and the lowest $\varepsilon_{Nd}(t)$ values (−18.1 to −17.7, Fig. 8). The corresponding two-stage Nd model

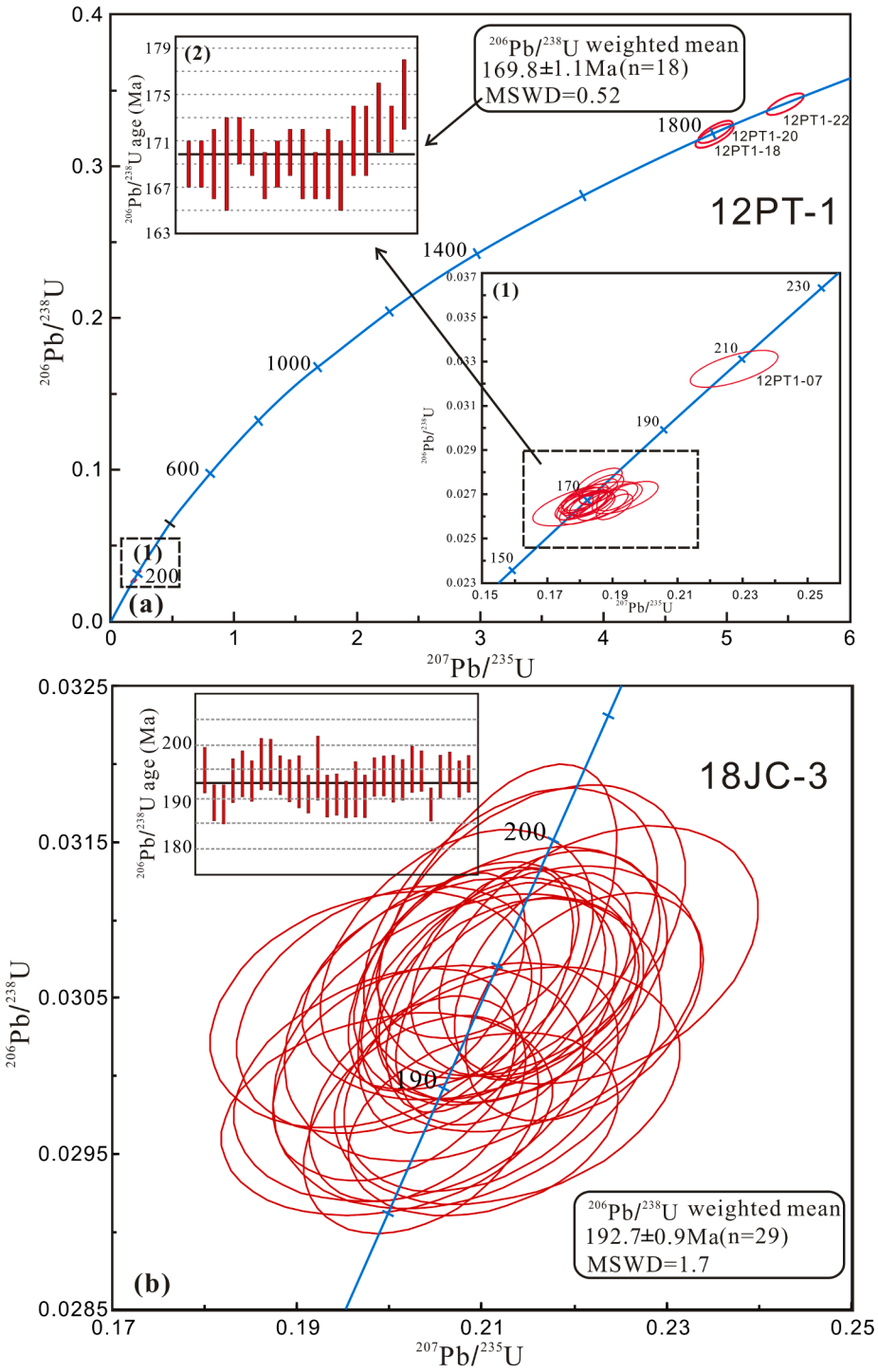

Fig. 5. Zircon U-Pb concordia diagrams and $^{206}Pb/^{238}U$ weighted mean ages for rocks from the Fanyindong (a) and Jincheng (b) plutons.

ages (T_{DM2}(Nd)) are strikingly older, ranging from 2.39 to 2.43 Ga. In contrast, the JC granites show significantly more depleted Sr–Nd isotopic compositions with I_{Sr} ratios of 0.7043–0.7044 and $\varepsilon_{Nd}(t)$ values of −0.7 to −1.2. The JC granites have relatively young two-stage Nd model ages (T_{DM2}(Nd) = 1.03–1.08 Ga). On the plot of $\varepsilon_{Nd}(t)$ vs. age (Fig. 8), the JC granites plot above the evolutionary trend defined by the Paleo- to Mesoproterozoic basement of the Cathaysia Block, whereas the FYD quartz diorite porphyries plot within the evolutionary domain of Precambrian basement in Cathaysia Block.

5.4. Zircon Lu–Hf isotopes

The zircon Hf isotopes were measured using the same grains used for U–Pb dating. The results are listed in Table 4 and illustrated in Fig. 9. Eighteen analyses on zircons from the FYD quartz diorite porphyry give relatively homogeneous Hf isotopic compositions with $\varepsilon_{Hf}(t)$ values ranging from −17.9 to −23.4. The corresponding two-stage Hf model ages (T_{DM2}) vary from 2.35 to 2.75 Ga. One analysis on a relict zircon core of Late Triassic U–Pb age yields low $\varepsilon_{Hf}(t)$ value of −23.8 with two-stage Hf model ages of 2.75 Ga. Three analyses on a relict zircon core with Paleoproterozoic U–Pb ages (1818–1903 Ma) give high $\varepsilon_{Hf}(t)$

Table 2
Major (wt.%) and trace element (ppm) compositions of the Fanyindong (FYD) and Jincheng (JC) plutons in southeast coast of China.

Pluton	Fanyindong						Jincheng					
Sample	12PT-1	03P-18#	03P-20#	P-6(1)	P8704-1	P8704-2	DS09-39–1*	DS09-39–2*	DS09-39–3*	18JC-2	18JC-3	18JC-4
Rock type	Quartz diorite porphyry						Biotite granite					
SiO_2	64.11	64.12	64.24	64.02	63.36	67.04	71.37	71.18	71.15	73.76	74.44	74.14
TiO_2	0.68	0.70	0.72	0.71	0.69	0.49	0.44	0.41	0.43	0.28	0.29	0.28
Al_2O_3	16.13	15.90	15.89	15.82	16.10	15.19	13.59	13.20	13.20	12.94	12.78	12.67
$Fe_2O_3^T$	5.04	4.95	5.10	4.99	5.55	3.95	3.42	4.33	4.14	2.60	2.86	2.66
MnO	0.08	0.07	0.08	0.08	0.12	0.11	0.06	0.05	0.06	0.03	0.04	0.04
MgO	2.44	1.98	2.05	1.99	2.12	1.30	0.68	0.79	0.71	0.37	0.40	0.37
CaO	3.83	5.08	3.96	3.97	4.41	2.95	1.75	1.53	1.69	1.33	1.32	0.83
Na_2O	3.62	2.77	3.40	2.78	3.19	4.11	3.16	3.05	3.15	3.12	3.10	3.00
K_2O	3.46	3.20	3.69	4.21	3.05	3.47	4.58	4.60	4.10	4.30	4.05	4.77
P_2O_5	0.15	0.13	0.14	0.14	0.14	0.12	0.14	0.12	0.11	0.07	0.08	0.07
LOI	1.26	0.97	1.25	1.13	0.76	0.89	0.64	0.53	1.04	0.31	0.49	0.47
Total	100.80	99.87	100.52	99.84	99.48	99.62	99.83	99.79	99.78	99.11	99.85	99.30
A/CNK	0.97	0.92	0.95	0.97	0.97	0.96	1.02	1.03	1.04	1.06	1.07	1.09
V	61.6	56.4	57.2	58.3						21.9	24.4	21.9
Sc	11.0	10.3	10.2	10.4						6.91	6.84	5.82
Ga	19.9	19.9	19.3	18.7			18.6	18.0	17.2	20.0	19.0	18.6
Cs	6.12	3.39	5.16	8.06						2.18	3.25	1.50
Rb	141	103	154	177			143	171	145	201	202	206
Ba	695	693	729	561			490	661	536	432	497	433
Th	20.3	21.9	19.7	19.1			31.9	14.4	12.6	28.9	21.7	25.6
U	5.16	5.01	4.86	4.73			3.94	2.27	2.92	4.25	3.93	3.50
Ta	1.10	1.15	1.11	1.11	0.86	0.69	0.78	1.15	1.41	2.04		
Nb	12.2	12.1	11.9	11.9	12.8	13.0	13.2	11.4	11.9	10.7		
Pb	24.7	28.9	27.5	36.7				9.64	9.26	10.9		
Sr	398	414	393	304	109	88.5	85.8	59.6	63.2	62.5		
Zr	156	143	187	190	92.4	76.5	113	190	164	180		
Hf	4.85	3.76	4.71	4.74	2.89	2.40	3.34	5.82	4.78	5.46		
Gd	5.75	5.08	4.77	4.54	10.3	5.78	5.02	7.58	6.02	6.01		
Y	19.4	20.4	15.7	17.9	48.7	38.7	38.2	63.1	44.3	40.2		
La	45.0	47.1	42.3	39.5	83.3	29.1	22.8	41.2	28.6	36.4		
Ce	84.0	78.6	72.7	69.0	158	56.3	44.4	77.9	51.7	65.7		
Pr	9.56	9.72	8.90	8.46	18.2	6.67	5.12	9.32	6.60	7.95		
Nd	38.6	36.0	32.8	31.7	69.0	26.3	21.2	35.0	22.8	26.5		
Sm	6.29	6.52	6.16	5.97	12.6	5.96	4.79	7.37	5.68	6.14		
Eu	1.36	1.33	1.26	1.02	1.11	1.05	0.90	0.68	0.68	0.62		
Gd	5.75	5.08	4.77	4.54	10.3	5.78	5.02	7.58	6.02	6.01		
Tb	0.79	0.76	0.73	0.68	1.71	1.13	1.04	1.35	1.05	1.03		
Dy	4.01	3.90	3.78	3.64	9.02	6.76	6.25	8.78	6.82	6.43		
Ho	0.71	0.75	0.75	0.69	1.63	1.29	1.21	1.86	1.41	1.33		
Er	2.03	1.90	1.83	1.76	4.96	4.01	3.96	5.20	3.99	3.69		
Tm	0.27	0.29	0.29	0.26	0.77	0.61	0.63	0.84	0.65	0.60		
Yb	1.75	1.80	1.78	1.64	4.53	3.78	4.01	5.19	4.10	3.76		
Lu	0.26	0.26	0.27	0.24	0.70	0.55	0.61	0.75	0.59	0.55		
t_{Zr} (℃)	761.2	749.7	774.8	779.4	737.2	723.8	755.9	805.7	794.7	804.4		

Note: LOI: loss on ignition; A/CNK = $Al_2O_3/(CaO + Na_2O + K_2O)$ (mol);t_{Zr} (℃), zircon saturation temperature.*Data from Liu et al. (2011).

values of −6.0 to −1.8, with T_{DM2} values of 2.85–2.65 Ga. In contrast, zircons from the JC biotite granites yield homogeneous, but significantly depleted, zircon Hf isotopic compositions, with $\varepsilon_{Hf}(t)$ values of +2.3 to +6.6. The corresponding two-stage Hf model ages (T_{DM2}) vary from 0.81 to 1.09 Ga.

6. Discussion

6.1. Petrogenesis of the FYD quartz diorite porphyries

The FYD quartz diorite porphyries have high Al_2O_3, low MgO, $Fe_2O_3^T$, Ni, Cr, Co, and V contents, and display significant depletions in HFSEs (High-field strength elements; e.g., Nb, Ta), and enrichment in LILEs and LREEs. The porphyries show extremely high radiogenic Sr isotope ratios and enriched bulk-rock Nd and zircon Hf isotopic compositions (I_{Sr} = 0.7184–0.7211, $\varepsilon_{Nd}(t)$ = −18.1 to −17.7, $\varepsilon_{Hf}(t)$ = −17.9 to −24.2). Their consistent crustal Nd (2.39–2.43 Ga) and Hf (2.35–2.75 Ga) model ages suggest that the porphyries mainly sourced from ancient crustal materials. In an age vs. ε_{Hf} (t) diagram (Fig. 9), all samples plot in the evolutionary trend defined by Paleoproterozoic granitoids and metamorphic rocks from the Badu complex considered to be the oldest rocks of the Cathaysia Block, Southeast China (Yu et al., 2012), indicating that the magmatic source of the FYD quartz diorite porphyries may be predominantly comprised of Palaeoproterozoic basement materials with a possible involvement of Neoarchean crustal materials. Four inherited zircons, three Paleoproterozoic ($^{207}Pb/^{206}Pb$ ages, ~1805–1903 Ma) and one Triassic ($^{206}Pb/^{238}U$ age, 207 Ma), within the FYD pluton show negative ε_{Hf} (t) values, and have overlapping two-stage Hf model ages of 2.65–2.85 Ga, similar to those of the magmatic zircons within the FYD pluton (2.35–2.75 Ga) and Paleoproterozoic granitoids and metamorphic rocks from the Badu complex (Fig. 9), further confirming that the FYD pluton mainly derived from reworking of the ancient basement rocks possibly with contributions of Archean crustal rocks, without significant input of juvenile material.

More importantly, the FYD quartz diorite porphyries are intermediate to slightly felsic, metaluminous, have typical I-type geochemical characteristics with low $10^4Ga/Al$ ratios (2.23–2.36) and the presence of amphibole. They have relatively low $Al_2O_3/(MgO + FeO^T)$ and $(Na_2O + K_2O)/(FeO^T + MgO + TiO_2)$ ratios, but high $CaO/(FeO^T + MgO + TiO_2)$ ratios, and all samples plot within the field defined by an experimental

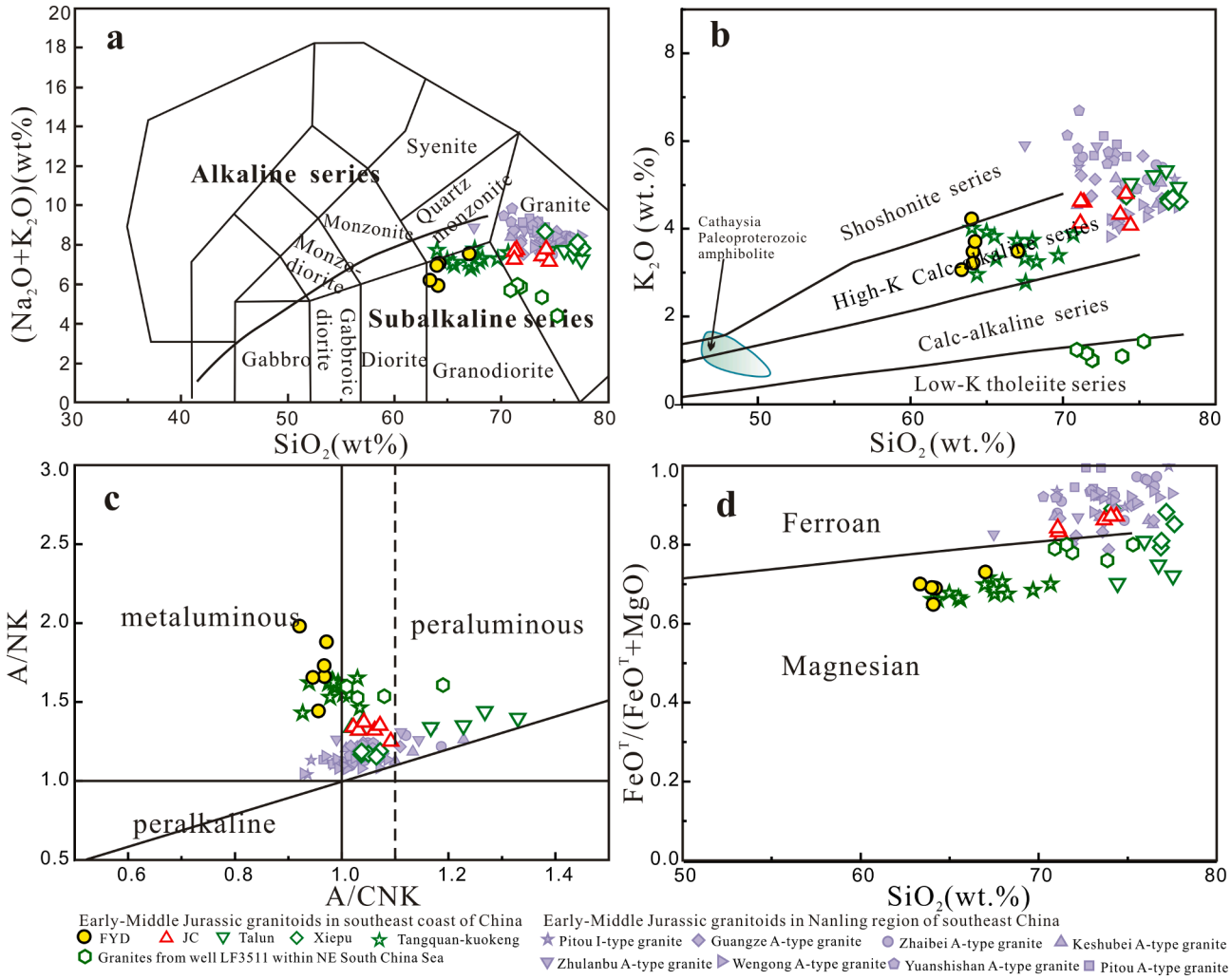

Fig. 6. Major elements classification of granitic rocks from the Fanyindong and Jincheng plutons, Southeast China. (a) Plot of $Na_2O + K_2O$ vs. SiO_2 (TAS) diagram (Middlemost, 1994; with the thick solid line from Irvine and Baragar,1971); (b) Plot of K_2O vs. SiO_2 diagram (Peccerillo and Taylor, 1976); (c) Plot of A/NK vs. A/CNK diagram (Chappell and White, 1974; Maniar and Piccoli, 1989); (d) Plot of $FeO^T/(FeO^T + MgO)$ vs. SiO_2 diagram (after Frost et al., 2001). The compositions of the Cathaysia Paleoproterozoic amphiboles are from Xia et al. (2012) and references therein. Data sources for the Early-Middle Jurassic granitoids in the Nanling region and southeast coast of China as in Fig. 1.

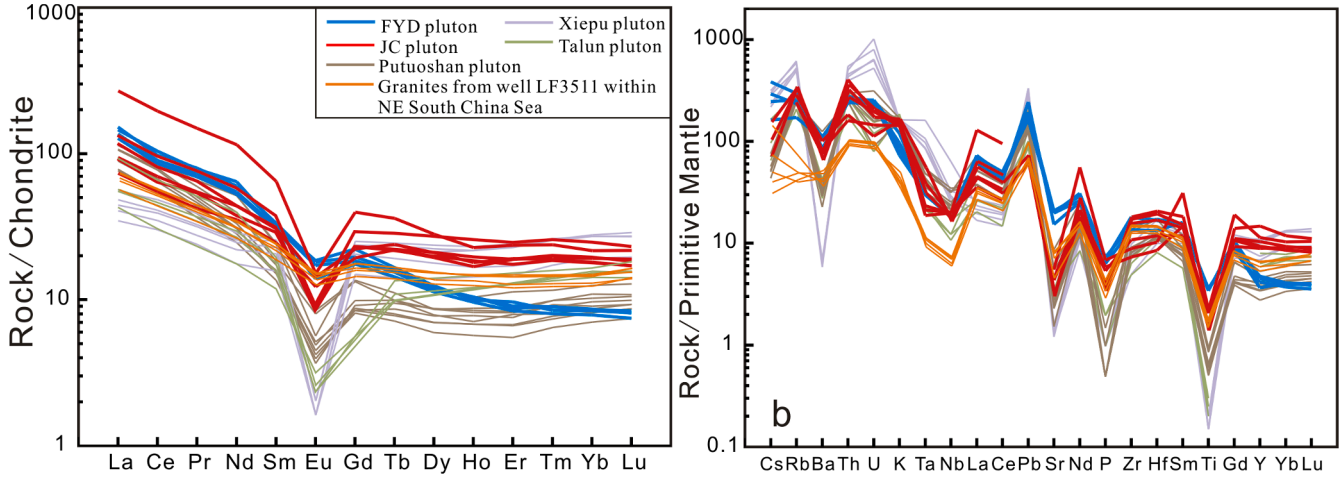

Fig. 7. Chondrite-normalized REE concentrations (a) and primitive-mantle-normalized trace element spider diagram (b) of rocks from the Fanyindong and Jincheng plutons. The normalization values for chondrite and primitive mantle are from Boynton (1984) and McDonough and Sun (1995), respectively. Data sources for the Early-Middle Jurassic granitoids in southeast China coast as in Fig. 1. Putuoshan granite data are from Zhao et al. (2016).

Table 3
Whole-rock Rb-Sr and Sm-Nd isotopic data for the Fanyindong (FYD) and Jincheng (JC) granitoids.

Sample no.	t(Ma)	Rb (ppm)	Sr (ppm)	$^{87}Rb/^{86}Sr$	$^{87}Sr/^{86}Sr$	$(^{87}Sr/^{86}Sr)_i$	Sm (ppm)	Nd (ppm)	$^{147}Sm/^{144}Nd$	$^{143}Nd/^{144}Nd$	$\varepsilon_{Nd}(t)$	T_{DM2}(Ga)
Fanyindong quartz diorite porphyry												
12PT-1	170	140.8	398.0	1.0254	0.723544 ± 2	0.721066	6.29	38.58	0.099	0.511624 ± 13	−17.66	2.39
P-6	170	177.4	303.5	1.6932	0.722459 ± 14	0.718367	5.97	31.70	0.114	0.511616 ± 12	−18.14	2.43
03P-18	170	102.9	413.9	0.7200	0.722679 ± 16	0.720939	6.52	35.99	0.109	0.511618 ± 13	−18.01	2.42
Jincheng biotite granite												
18JC-2	193	200.6	59.6	9.7528	0.731059 ± 7	0.704293	7.37	35.02	0.127	0.512514 ± 5	−0.71	1.03
18JC-3	193	201.6	63.2	9.2500	0.729766 ± 6	0.704380	5.68	22.76	0.151	0.512517 ± 5	−1.23	1.08

$\varepsilon_{Nd}(t)$ values are calculated by granitoid ages and based on ^{147}Sm decay constant of 6.54×10^{-12}, the $^{143}Nd/^{144}Nd$ and $^{147}Sm/^{144}Nd$ ratios of chondrite and depleted mantle at present day are 0.512630 and 0.1960, 0.513151 and 0.2136, respectively (Miller and O'Nions, 1985). T_{DM2} ages are calculated according to the two-stage model as presented by Wu et al. (2000).

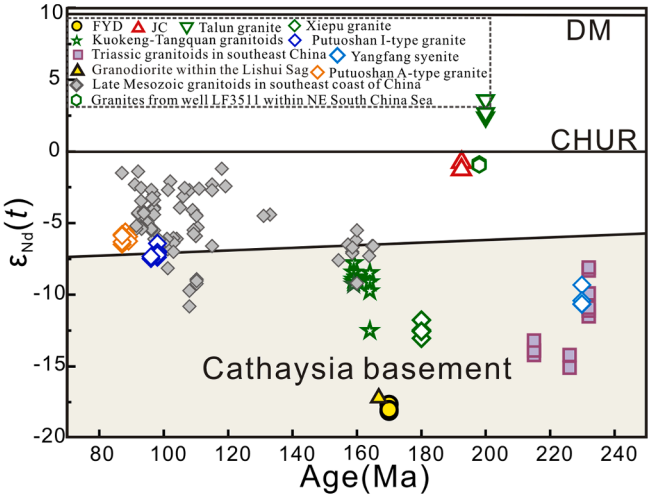

Fig. 8. Age vs. ε_{Nd}(t) values of the Mesozoic granitoids from the SE China. The area of Cathaysia basement is modified from Chen and Jahn (1998). The data for the Late Mesozoic granitoids in the coastal area of SE China are from Yang et al. (2018), Li et al. (2014b), Chen et al. (2017) and references therein. The data for the Triassic granitoids in SE China are from Mao et al. (2013), Li et al. (2012c) and Xia et al. (2012). The data for the Yangfang syenite are from Wang et al. (2005). The data for the granodiorite within the Lishui Sag of the East China Sea Basin are from Chen et al. (2005). Data sources for the Early-Middle Jurassic granitoids in coastal area of southeast China as in Fig. 1.

melt generated from meta-mafic and/or meta-tonalitic rocks in the source discrimination diagrams (Fig. 10). We thus suggest that the source candidates for the FYD quartz diorite porphyries are mainly basaltic, with subordinate intermediate igneous rocks. Studies of experimental dehydration melting provide evidence that source rocks for K-rich melts seem to be more potassic than sources of K-poor, intermediate to acidic magma (Sisson et al., 2005). Abundant intermediate-mafic igneous rocks have been identified in the lowest part of the Tangyuan Formation, Badu complex. Zircon U–Pb ages obtained for some granitoids (e.g., Tianhou, Xiaji and Danzhu granitic plutons) intruding the Badu Complex suggest that the Badu complex formed before the late Paleoproterozoic (Yu et al., 2012). Available geochemical data for these amphibolites in the Badu complex indicates that these rocks usually have medium to high K_2O contents, suggesting widespread existence of K-rich intermediate-mafic rocks in the Cathaysia basement (Fig. 6b). These proposed K-rich, intermediate-mafic rocks of the ancient basement in the Cathaysia Block may be potential sources for the FYD quartz diorite porphyries.

Alternatively, the FYD quartz diorite porphyries are characterized by relatively depleted HREEs and Y (15.7–20.4 ppm) contents with elevated La/Yb (23.8–26.2) and Sr/Y (17.0–25.1), have the geochemical affinities of adakitic rocks (Fig. 11). HREEs (e.g., Yb, Lu) are strongly compatible with garnet, and MREEs (e.g., Gd, Dy, Ho) are compatible with amphibole. When garnet is the main residual mineral, HREEs will show strongly fractionated patterns with Y/Yb > 10 and $(Ho/Yb)_N$ > 1.2. When amphibole is the main residual mineral, the resultant melts will show flat REE patterns with Y/Yb≈10 and $(Ho/Yb)_N$≈1 (Ge et al., 2002). The FYD quartz diorite porphyries have Y/Yb and $(Ho/Yb)_N$ values of 8.9–11.3 (average = 10.5) and 1.18–1.23 (average = 1.21), respectively. They also show strongly fractionated HREE patterns with $(Dy/Yb)_N$ values of 1.38–1.49 (Fig. 7a). Moreover, their Sm/Yb ratios (3.46–3.64) are distinctively higher than those of the coexisting Putuoshan alkali-feldspar granites (1.41–2.03, Zhao et al., 2016) and Early Jurassic granitic rocks (0.71–2.78) within the southeast coast of China (Li et al., 2012a; Liu et al., 2011; Xu et al., 2017; Yui et al., 2017). Experimental studies demonstrate that partial melting of mafic lower crust at 800–900℃ and a pressure of about 1.0–1.5 GPa can generate adakite-like melts with garnet amphibolite or garnet granulite residues (Qian and Hermann, 2013), geochemically similar to those of the FYD pluton. It is thus suggested that the FYD pluton was generated by melting of a thickened lower crust with garnet remaining as a residual mineral in the source. Notably, the FYD quartz diorite porphyries have slightly higher Y (15.69–20.40 ppm) but lower Sr (303.5–413.9 ppm) concentrations than those of typical adakites (Y ≤ 18 ppm, Sr mainly >400 ppm, Defant and Drummond, 1990). These data indicate that amphibole, rather than garnet, occurs as the major residual phase in the source of the porphyries. Combined with weak depletions in Eu, Ba and Sr, these suggest that the magmatic source of the FYD pluton may not be as deep as typical adakite sources, and amphibole, as well as minor plagioclase and garnet, occur as the residual phases.

In summary, we propose that the FYD quartz diorite porphyries were generated by partial melting of ancient medium- to high-K_2O intermediate-mafic rocks in deep crust where amphibole, minor garnet and plagioclase are stable in the residue. The FYD quartz diorite porphyries with ca. 2.35–2.75 Ga crustal Nd–Hf model ages, as well as the inherited zircons with two-stage Hf model ages of 2.65–2.85 Ga, allude to the existence of Archean basement beneath the Cathaysia Block. Consequently, we suggest that the ancient basement rocks similar to the Badu complex are also distributed within the deep crust beneath the southeast coast of China, though most of the Palaeoproterozoic-Neoarchean basement materials have been recycled or reworked by extensive tectono-thermal events, especially during the Mesozoic (Xu et al., 2007; Zhou et al., 2006).

6.2. *Petrogenesis of the JC biotite granites*

The biotite granites from the JC pluton are highly siliceous, calc-alkaline, and have typical I-type geochemical characteristics with no observed cogenetic mafic rocks. They are marked by significantly negative Nb–Ta anomalies in the primitive-mantle-normalized multi-element variation patterns (Fig. 7), low MgO, $Fe_2O_3^T$, and MnO concentrations, and low Mg# values (21.8–28.5). These data, coupled with the absence of intermediate rocks in the Jincheng region, indicate that

Table 4
In-situ Hf isotopic compositions of zircons from the Fanyindong (FYD) and Jincheng (JC) granitoids.

Spot	Age (Ma)	$^{176}Lu/^{177}Hf$	$^{176}Hf/^{177}Hf$	2σ	$^{176}Yb/^{177}Hf$	$(^{176}Hf/^{177}Hf)_i$	$\varepsilon_{Hf}(t)$	2σ	T_{DM1}(Ga)	T_{DM2}(Ga)
Fanyindong quartz diorite porphyry										
12PT1-1	170	0.000623	0.28209	0.000034	0.019388	0.282088	−20.5	1.2	1.62	2.51
12PT1-2	170	0.000573	0.281993	0.000022	0.018836	0.281991	−23.9	0.8	1.75	2.73
12PT1-3	170	0.000682	0.282083	0.000021	0.021759	0.282080	−20.7	0.7	1.63	2.53
12PT1-4	170	0.000867	0.281984	0.000044	0.029021	0.281981	−24.2	1.6	1.78	2.75
12PT1-5	170	0.001214	0.28201	0.000027	0.043034	0.282006	−23.4	0.9	1.76	2.69
12PT1-6	170	0.000732	0.282081	0.000027	0.024951	0.282079	−20.8	1.0	1.64	2.53
12PT1-7	207	0.000799	0.281974	0.000022	0.026724	0.281971	−23.8	0.8	1.79	2.75
12PT1-8	170	0.000508	0.282057	0.000023	0.016604	0.282055	−21.6	0.8	1.66	2.58
12PT1-9	170	0.00059	0.282094	0.000033	0.021338	0.282092	−20.3	1.2	1.61	2.50
12PT1-10	170	0.000614	0.282038	0.000031	0.01971	0.282036	−22.3	1.1	1.69	2.63
12PT1-11	170	0.000809	0.282041	0.000024	0.027744	0.282039	−22.2	0.9	1.70	2.62
12PT1-12	170	0.000902	0.282032	0.000029	0.031045	0.282029	−22.6	1.0	1.71	2.64
12PT1-13	170	0.001217	0.282164	0.000028	0.043021	0.282160	−17.9	1.0	1.54	2.35
12PT1-14	170	0.000571	0.282074	0.000021	0.017179	0.282072	−21.0	0.7	1.64	2.55
12PT1-15	170	0.000543	0.282089	0.000022	0.016389	0.282087	−20.5	0.8	1.62	2.51
12PT1-16	170	0.000755	0.282052	0.000029	0.023703	0.282049	−21.8	1.0	1.68	2.60
12PT1-17	170	0.000897	0.282114	0.000024	0.032229	0.282111	−19.7	0.9	1.60	2.46
12PT1-18	1818	0.00121	0.281498	0.000029	0.040353	0.281456	−6.0	1.0	2.47	2.85
12PT1-19	1903	0.000633	0.281545	0.000019	0.020733	0.281522	−1.7	0.7	2.37	2.65
12PT1-20	1805	0.000495	0.281524	0.000024	0.01559	0.281507	−4.5	0.8	2.39	2.75
12PT1-21	170	0.000512	0.282052	0.000036	0.016242	0.282051	−21.8	1.3	1.67	2.59
Jincheng biotite granite										
18JC-3-01	192.7	0.001264	0.282778	0.000014	0.040267	0.282773	4.3	0.5	0.68	0.96
18JC-3-02	192.7	0.001704	0.282762	0.000015	0.054504	0.282756	3.7	0.5	0.71	1.00
18JC-3-03	192.7	0.001645	0.282784	0.000013	0.052204	0.282778	4.4	0.5	0.68	0.95
18JC-3-04	192.7	0.001335	0.282784	0.000013	0.041487	0.282779	4.5	0.4	0.67	0.95
18JC-3-05	192.7	0.001893	0.282769	0.000012	0.058852	0.282762	3.9	0.4	0.70	0.99
18JC-3-06	192.7	0.004074	0.282760	0.000016	0.134786	0.282745	3.3	0.6	0.76	1.02
18JC-3-07	192.7	0.002546	0.282772	0.000013	0.076857	0.282763	3.9	0.5	0.71	0.98
18JC-3-08	192.7	0.001124	0.282774	0.000014	0.035916	0.282769	4.1	0.5	0.68	0.97
18JC-3-09	192.7	0.002875	0.282800	0.000017	0.090206	0.282790	4.9	0.6	0.67	0.92
18JC-3-10	192.7	0.001636	0.282799	0.000016	0.047203	0.282793	5.0	0.5	0.65	0.92
*1	192.7	0.002051	0.282785	0.000013	0.113864	0.282778	4.4	0.5	0.68	0.95
*2	192.7	0.001536	0.282723	0.000014	0.086362	0.282717	2.3	0.5	0.76	1.09
*3	192.7	0.002508	0.282753	0.000017	0.152742	0.282744	3.2	0.6	0.74	1.03
*4	192.7	0.003036	0.282781	0.000013	0.181621	0.282770	4.2	0.5	0.71	0.97
*5	192.7	0.002296	0.282847	0.000013	0.136375	0.282839	6.6	0.5	0.59	0.81
*6	192.7	0.003211	0.282734	0.000018	0.187869	0.282722	2.5	0.6	0.78	1.08
*7	192.7	0.002732	0.282738	0.000017	0.139114	0.282728	2.7	0.6	0.76	1.06
*8	192.7	0.001762	0.282796	0.000017	0.096991	0.282790	4.9	0.6	0.66	0.92
*9	192.7	0.003033	0.282745	0.000017	0.173806	0.282734	2.9	0.6	0.76	1.05

For the calculation of $\varepsilon_{Hf}(t)$ values, we adopted the ^{176}Lu decay constant of 1.867×10^{-11} (Soderlund et al., 2004), the present-day chondritic values of $^{176}Lu/^{177}Hf = 0.0332$ and $^{176}Hf/^{177}Hf = 0.828772$ (Blichert-Toft and Albarède, 1997). To calculate one-stage model ages (T_{DM1}) relative to a depleted-mantle source, we have adopted the present-day depleted-mantle values of $^{176}Lu/^{177}Hf = 0.0384$ and $^{176}Hf/^{177}Hf = 0.28325$ (Vervoort and Blichert-Toft, 1999). To calculate two-stage model ages (T_{DM2}), we adopted an assumed $^{176}Lu/^{177}Hf$ ratio of 0.015 for the average continental crust (Griffin et al., 2006). *Data for the Jincheng biotite granite are from Liu et al. (2011).

the JC granites derived from partial melting of a crustal source, rather than fractional crystallization of a mantle-derived basaltic magma. Although evidence of Meso- to Neoproterozoic mafic magmatism is observed in the Wuyi region of the western Fujian Province, with zircon Hf isotopic compositions ($\varepsilon_{Hf}(t) = +4.1$ to $+10.5$; $T_{DM2} = 0.89$–1.45 Ga) similar to the JC granites ($\varepsilon_{Hf}(t) = +2.3$ to $+6.6$; $T_{DM2} = 0.81$–1.09) (Shu et al., 2011), no Precambrian intermediate-mafic igneous rocks are reported in the southeast coast of China, especially in the Jincheng region. Detailed U–Pb dating and Lu–Hf analyses of detrital zircons from basement metamorphic rocks within SE China has revealed five main episodes of juvenile crust generation at 3.6 Ga, 2.8 Ga, 2.6–2.4 Ga, 1.85 Ga and 0.8–0.7 Ga (Yu et al., 2010). The calculated Nd and Hf model ages (0.82–1.08 Ga) of the JC granites are inconsistent with any previously reported episodes of crust generation. Therefore, it seems unlikely that partial melting of Neoproterozoic magmatic rocks produced the JC granites.

It is important to note that the Sr–Nd–Hf isotope compositions of the JC biotite granites ($I_{Sr} = 0.7043$–0.7044, $\varepsilon_{Nd}(t) = -0.7$ to -1.2, $\varepsilon_{Hf}(t) = +2.3$ to $+6.6$) are significantly depleted relative to the Mesozoic granitoids within southeast China (Figs. 9 and 12). All of the JC granite samples plot above the evolutionary trend defined by the ancient basement of the Cathaysia Block (Figs. 8 and 9), indicating involvement of a depleted mantle-derived component during their generation. Depleted Sr–Nd–Hf isotopic ratios are commonly interpreted to be caused by significant input of depleted mantle materials or by partial re-melting of juvenile crust (Li et al., 2012b; Qiu et al., 2012; Wong et al., 2009). More recent studies have used integrated field and petrographic observation, as well as geochemical and *in-situ* zircon U–Pb, Hf, and O isotopic data to demonstrate that I-type granitoids within southeast China likely formed by mixing of crustal- and mantle-derived magmas (Chen et al., 2013b; Zhao et al., 2016). The identification of the FYD pluton ($\varepsilon_{Nd}(t) = -18.1$ to -17.7, $I_{Sr} = 0.7184$–0.7211) within the Zhoushan Archipelago and the c. 167 Ma granodiorite within the Lishui Sag of the East China Sea Basin ($\varepsilon_{Nd}(t) = -17.0$, $I_{Sr} = 0.716$, Chen et al., 2005) with highly evolved isotopic character further confirms the presence of an ancient crustal basement beneath the southeast coast of China. However, if the JC granites formed by direct partial melting of these crustal basement rocks similar to the Badu complex, large amounts of mantle-derived depleted magma should have been involved. A simple, two-end-member modeling calculation is employed here to evaluate the origin of the JC pluton. The FYD quartz diorite porphyries in this study are used to represent the crustal end-member, and the Ningyuan

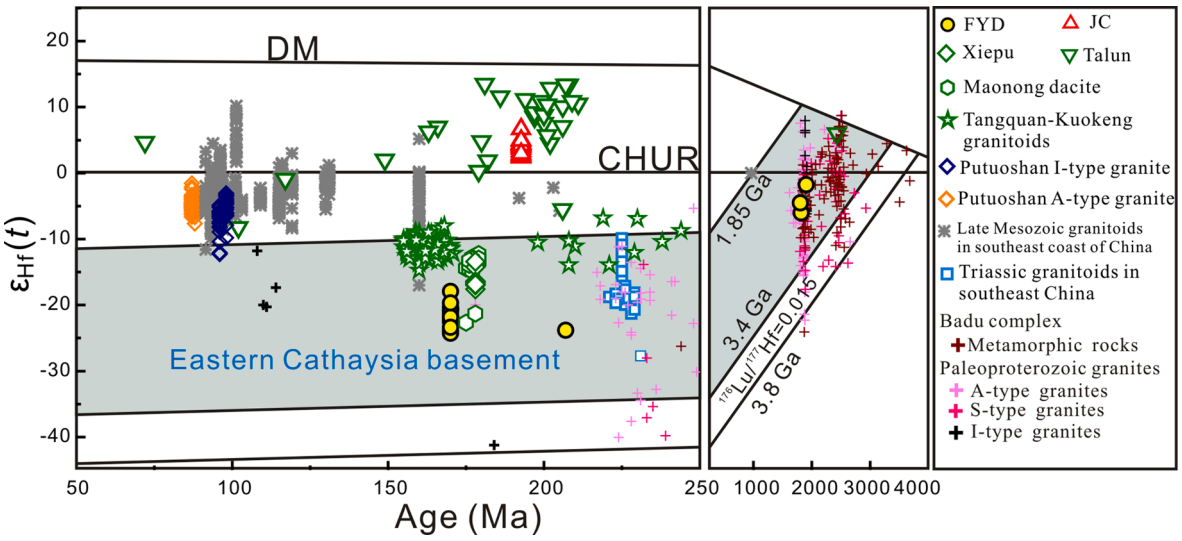

Fig. 9. Hf-isotope compositions of representative zircons from Fanyindong and Jincheng granitic rocks. The area of Eastern Cathaysia basement is after Xu et al. (2007). The data for the Badu complexes, and Paleoproterozoic A-type, I-type and S-type granites are after Xia et al. (2012), Liu et al. (2014), Yu et al. (2012) and references therein. Data sources for Mesozoic granitoids in southeast China as in Fig. 8.

basalts from the southern Hunan Province were selected to represent the depleted mantle (Li et al., 2004). Our calculations show that nearly 80% of the mantle-derived materials must be mixed to generate the JC granites (Fig. 12). Considering that addition of 80% mantle-derived melts would make the final magma basaltic rather than highly siliceous, it is likely that the parental magma of JC pluton was not generated by mixing of mantle-derived material with crustal-derived magmas that formed by partial melting of the ancient basement rocks similar to the Badu complex. The JC granites have indistinctive Sr–Nd–Hf isotopic variation (Figs. 8 and 9), suggesting that magma mixing between felsic and basaltic magmas is not a reasonable hypothesis for the formation of the JC granites (Kemp et al., 2005). Additionally, the absence of observed mafic, microgranular enclaves and petrographic disequilibrium textures in the JC granites lends further support to the idea that they did not form by mafic and felsic magma mixing (Chen et al., 2013a; Liu et al., 2013).

Alternatively, Li et al.(2012b) suggests that the Cretaceous Quanzhou and Huacuo granites within the coastal Fujian Province were derived from partial melting of juvenile crust with a mixed lithology. This type of origin has been widely reported for granitoids in Eastern China, which is the easternmost part of the Central Asian Orogenic Belt, NE China (Wu et al., 2003), and the eastern segment of the Jiangnan Orogen (Zheng et al., 2008). More importantly, the Cretaceous Putuoshan I- and A-type granites, which spatially coexist with the FYD pluton (Fig. 2b), show relatively depleted Nd–Hf isotope compositions with SiO_2 contents of 75.75–77.50 wt% (Zhao et al., 2016). The significant difference in isotope composition between the FYD granitoid and Putuoshan I- and A-type granites, as well as most of the Late Mesozoic granitoids within the coastal area of Southeast China (Figs. 8 and 9), further indicates that partial melting of a mixed source rock comprised of depleted mantle-derived basic rocks and crustal components for the formation of granitoids within southeast China coast should be ubiquitous. A compilation of available Nd and zircon Hf isotopic data for Mesozoic granitoids within Southeast China indicates that their $\varepsilon_{Nd}(t)$ and zircon $\varepsilon_{Hf}(t)$ values have a linear trend, which gradually increases with progressive younger ages for the Mesozoic granitoids (Figs. 8 and 9). This indicates that the magma sources for most of the Late Mesozoic granitoids experienced significant input of mantle-derived juvenile materials during the Mesozoic. Similarly, the systematic Hf isotopic values for the detrital zircons suggest that the eastern Cathaysia Block rarely experienced crustal growth from the Mesoproterozoic to Early Mesozoic (Xu et al., 2007). Thus, the ancient basement rocks in southeast China must have been modified, mainly, during the multi-stage Mesozoic magmatism (Wong et al., 2009). This process not only recycled old basement, but also continuously contributed significant input of mantle-derived juvenile materials during the Mesozoic. This resulted in gradual modification and vertical growth of the pre-existing lower crust beneath the coastal area of southeast China (Chen et al., 2017; Li et al., 2020). This resultant juvenile lower crust could provide potential source rocks with relatively depleted Sr–Nd–Hf isotopic compositions for generation of the following granitic rocks in southeast coast of China.

The presence of inherited zircon cores ($^{207}Pb/^{206}Pb$ age = 2423 Ma) within the JC biotite granite (Liu et al., 2011) indicates that an inherited component from crustal rocks, similar to those within the Badu complex, might be involved during generation of the granite. These data, combined with the relatively depleted and uniform whole-rock Sr–Nd and zircon Hf isotopic compositions, indicate that the granite derived from a mixed source comprised of a high proportion of depleted mantle with some ancient crustal components. Moreover, the JC granites are K-rich (Fig. 6b), show some features transitional between S-type and normal I-type granites with the A/CNK values ranging from 1.02 to 1.09, and the A/CNK values increase with decreasing MgO, FeO^T and TiO_2 contents. These data can be ascribed to the input of metasedimentary material during their formation (Zhao et al., 2015). Several experimental studies have shown that compositional differences of magmas formed by partial melting of different source regions under variable melting conditions could be differentiated in terms of molar $Al_2O_3/(MgO + FeO^T)$ and K_2O/Na_2O ratios (Altherr et al., 2000 and references therein). These melts derived from intermediate-mafic meta-igneous rocks have lower molar $Al_2O_3/(MgO + FeO^T)$ and K_2O/Na_2O ratios than those derived from metapelites and metagreywackes. The JC granites show higher values of $Al_2O_3/(MgO + FeO^T)$ and K_2O/Na_2O than the FYD granitoids. There exists a positive relationship between $Al_2O_3/(MgO + FeO^T)$ and A/CNK values. In the source discrimination diagram, the JC granites plot in the transitional field between *meta*-sedimentary rocks and *meta*-igneous rocks (Fig. 10). These confirm a significant contribution of sedimentary components to the origin of JC biotite granites. The protoliths of the metamorphic rocks of the Badu Complex were predominantly composed of sedimentary rocks and volcaniclastic rocks (Yu et al., 2012), which further suggests that the JC granites were likely derived from partial melting of juvenile crust of a mixed lithology formed by pre-existing metasedimentary rocks underplated by mantle-derived mafic magma. This hypothesis is supported by the highly evolved character of the JC

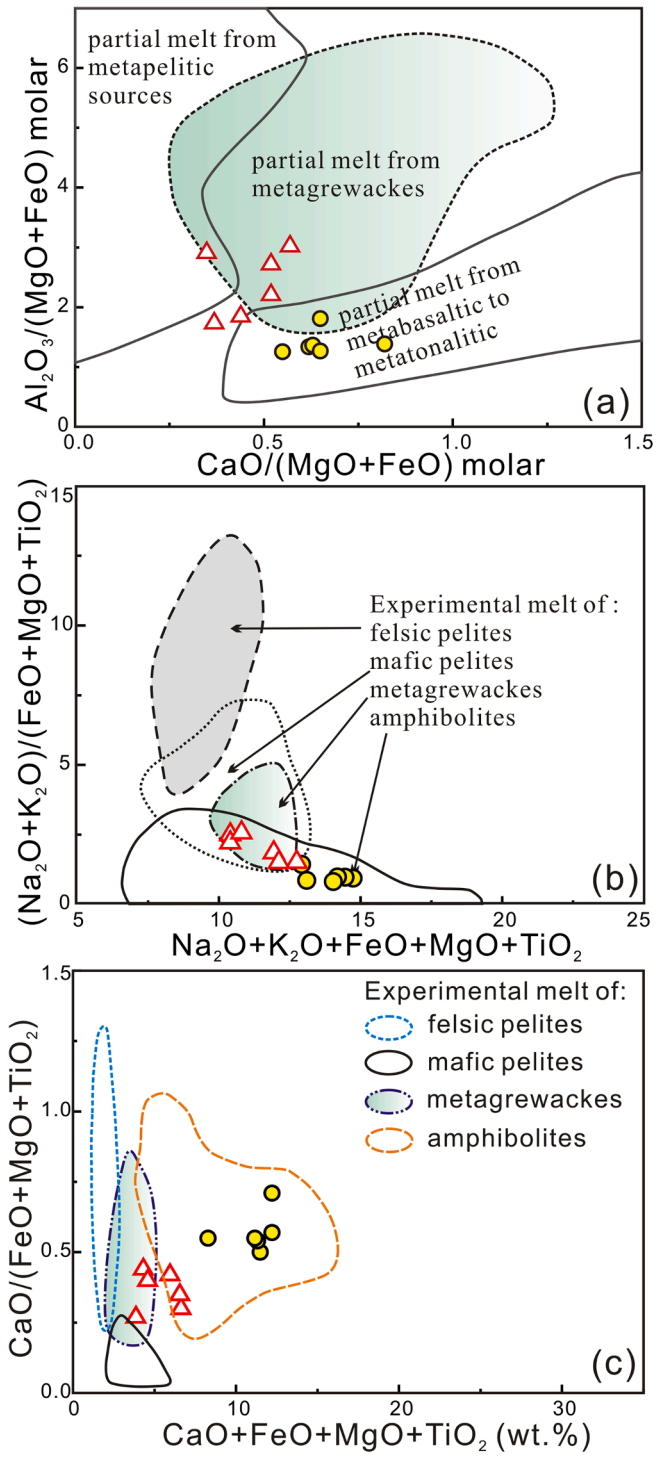

Fig. 10. Source discrimination diagrams for Fanyindong and Jincheng granitoids. (a) CaO/(MgO + FeO) molar vs. Al_2O_3/(MgO + FeO) molar diagram (modified after Altherr et al., 2000). (b) $Na_2O + K_2O + FeO + MgO + TiO_2$ vs. $(Na_2O + K_2O)/(FeO + MgO + TiO_2)$ diagram and (c) Al_2O_3/TiO_2 vs. CaO/Na_2O diagram (modified after Patiño Douce, 1999). Symbols are the same as in Fig. 6.

biotite granites (SiO_2 = 71.15–74.44 wt%) because a juvenile mantle-derived mafic crust is too mafic to produce such a felsic melt (Niu et al., 2013).

The JC biotite granites have high Y and Yb contents, low Sr/Y, Sm/Yb and La/Yb, show flat HREE patterns, and have significantly negative Eu, Ba and Sr anomalies (Fig. 7). These characteristics suggest that they were generated from sources containing residual plagioclase but lacking

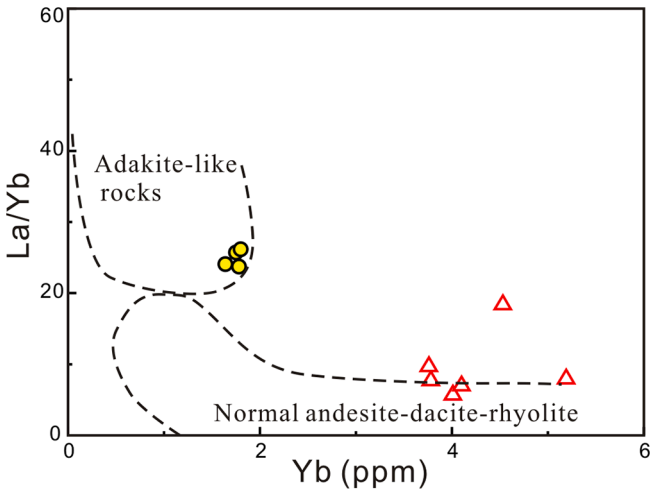

Fig. 11. La/Yb versus Yb diagram for the Fanyindong and Jincheng plutons. The fields of adakite-like rocks and normal andesite-dacite-rhyolite are from Richards et al. (2012). Symbols are the same as in Fig. 6.

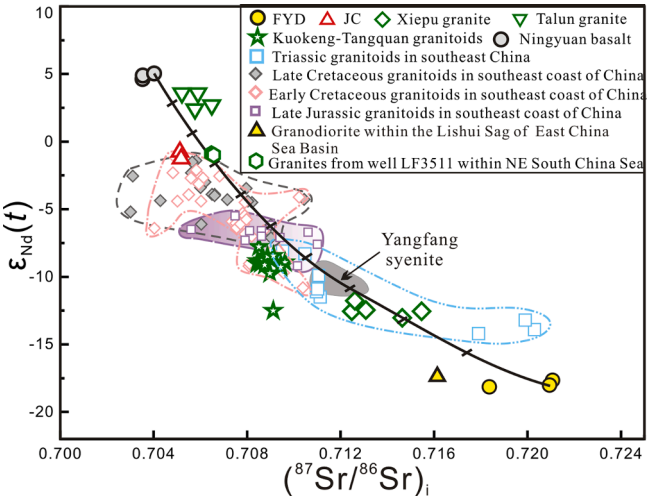

Fig. 12. Whole-rock $\varepsilon_{Nd}(t)$ vs. $(^{87}Sr/^{86}Sr)_i$ diagram for the Fanyindong and Jincheng plutons. Black line is a calculated binary mixing curve between possible mafic and felsic magma end-members. Depleted mantle is represented by the Ningyuan basalt in Hunan Province (Li et al., 2004). Lithospheric mantle is represented by the Yangfang aegirine–augite syenite in western Fujian Province (Wang et al., 2005). The crustal end-member is represented by the Fanyindong quartz diorite porphyry in this study. Tick marks represent 10% mixing increments. Data sources for the Mesozoic granitoids in southeast China as in Fig. 8.

garnet, implying a relatively shallow magma depth. These results lead to the interpretation that the JC granites were produced by the partial melting of mixed source rocks, with plagioclase-rich residual phases in the lower crust, followed by variable degrees of differentiation. Furthermore, combining this new data with previous studies, lends to the recognition that underplating of mantle-derived mafic magma, especially during the Mesozoic, exerted a significant role in modification of the pre-existing ancient lower crust, and gave rise to the formation of this relatively juvenile source region in the lower crust. Variations in isotopic compositions of the Mesozoic granitoids in SE China are mainly controlled by different proportions of mantle-derived mafic rock and ancient basement rocks in their source, as well as the subsequent magma processes that are possible, such as magma mixing and crustal assimilation (Chen et al., 2017; Qiu et al., 2012).

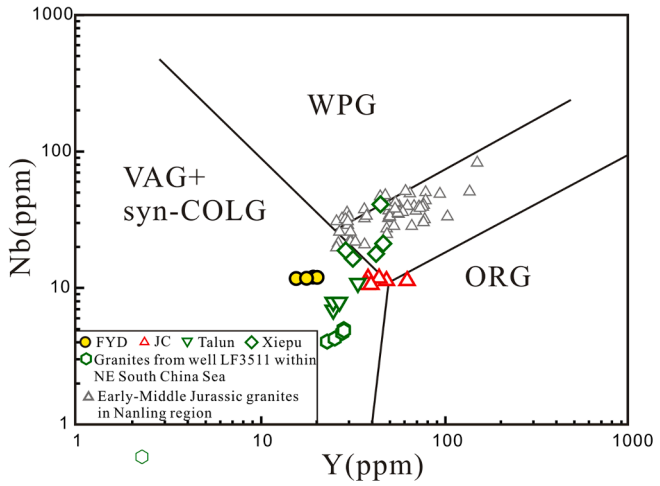

Fig. 13. Tectonic discrimination diagram of Pearce et al. (1984) showing the possible tectonic setting for the Early-Middle Jurassic granitoids in southeast coast of China. VAG–volcanic-arc granite, Syn-COLG–*syn*-collision granite, WPG–within-plate granite, ORG–ocean-ridge granite. Data sources for the Early-Middle Jurassic granitoids in southeast China as in Fig. 6.

6.3. *Implications for the Mesozoic tectonic evolution of South China*

Numerous studies have shown that the Early–Middle Jurassic igneous rocks within southeast China are predominantly concentrated within the Nanling region (Fig. 1). Although the igneous rocks within the Nanling region have been widely studies in the past, the tectonic settings in which these Jurassic igneous rocks formed remain highly controversial. Debates have focused on the initial timing of the Paleo-Pacific Plate subduction and the geodynamic mechanism responsible for generation of the Mesozoic magmatic rocks in southeast China. The under-studied Early–Middle Jurassic magmatic rocks within the southeast coast of China thus provide ideal samples for determining the Late Mesozoic geodynamic evolution of southeast China.

6.3.1. *The initiation time of Paleo–Pacific plate subduction beneath the South China Block*

Constraining the timing of subduction initiation for the Paleo-Pacific Plate beneath the South China block is essential for deciphering the timing of the Mesozoic tectonic transition from the Tethys orogenic regime to the Paleo-Pacific regime. Enrichments in LILEs (e.g., K, Rb), and LREEs, and depletions in HFSEs (e.g., Nb and Ta), correlate both the FYD and JC plutons with an arc-like geochemical affinity (Fig. 7). These geochemical characteristics are similar to those of the Talun granite in Taiwan (ca. 200 Ma, Yui et al., 2017) and Xiepu granite in coastal Zhejiang (180 Ma, Li et al., 2012a), as well as the granites from well LF3511 within NE South China Sea (ca. 198 Ma, Xu et al., 2017) (Fig. 7). The majority of the samples from these Early–Middle Jurassic igneous rocks within the southeast coast plot within the field of volcanic arc granites using the Y–Nb discrimination diagram (Fig. 13), which supports a subduction zone origin. Additionally, the occurrence and stability of euhedral hornblende and biotite crystals in the FYD pluton indicate oxidized and H_2O-rich conditions, which are characteristics of arc magmatism (Zhu et al., 2013). Inherited zircon grains of Paleoproterozoic-age (Fig. 9) and Sr–Nd–Hf isotopic compositions for the FYD, JC, Maonong, Xiepu and Talun magmatic rocks and the Early Jurassic granites from well LF3511(Liu et al., 2011; Liu et al., 2012; Xu et al., 2017; Yui et al., 2017) further support a continental arc origin. It is therefore suggested that these Early–Middle Jurassic magmatic rocks formed in an active continental margin setting, and spatially constitute a NE-trending, Early–Middle Jurassic arc-related magmatic rock belt along the southeast coast of China (Fig. 1, SE coastal belt), which parallels the convergence boundary between the Paleo-Pacific plate and South China Block. Geochemical features and spatial distribution of these Early–Middle Jurassic magmatic rocks along the coast strongly suggest~~s~~ that the Pacific tectonic domain, rather than Tethys tectonic domain, was responsible for generation of the Early Jurassic igneous rocks in southeast China. The subduction of the Paleo-Pacific plate thus had been initiated, at latest, by the Early Jurassic.

The typical flat-slab subduction and subsequent slab-foundering model proposed by Li and Li (2007) fails to explain the coexistence of an Early–Middle Jurassic, nearly E–W trending, Nanling belt with ~500 km length and an Early–Middle Jurassic, NE-trending, SE coastal belt, in the Cathaysia Block (Fig. 1). Moreover, slab break-off and foundering could induce a linear heat abnormality parallel to the subduction zone, corresponding to a narrow, linear zone of magmatism of limited extent (Davies and von Blanckenburg, 1995). This is not what is observed in the geologic record of southeast China. A recent study proposed that Late Permian–Early Triassic arc granites and volcanic rocks including the Wuzhishan pluton, are widely spread in the southeastern Guangxi and Hainan Provinces, and ascribed their formation to the northward subduction of the eastern Paleo-Tethys, rather than the subduction of the Paleo-Pacific plate (Li et al., 2016b). Therefore, the subduction of the Paleo-Pacific plate under the South China Block is unlikely to have occurred as early as the Late Permian–Early Triassic, as proposed by Li and Li (2007).

Identification of several 180–205 Ma intrusions in the SE coastal belt, including the JC, Xiepu, and Talun granites along the coast (Yui et al., 2017; Zhou et al., 2018), suggests that igneous activity during the Early Jurassic may have been more continuous than what previously proposed by Zhou et al. (2006), which hypothesized that there was a magmatic lull between 180 and 205 Ma. Nevertheless, only minor Early–Middle Jurassic magmatic rocks are exposed along the southeast China coast, indicating that the influence of the Paleo-Pacific plate on the Cathysia Block is relatively weak, which seems to imply generation during the early stages of subduction (Liu et al., 2012). Geochemically, the Early Jurassic Talun, JC, and Xiepu granites within the SE coastal belt, as well as granites from well LF3511, have relatively low Eu/Eu* ratios and Sr and Ba contents, and show significantly low La/Yb, Sr/Y, and Gd/Yb ratios (Fig. 14), indicating that the parental magma of these Early Jurassic rocks originated from a relatively shallow source, at depths where plagioclase is stable. In contrast, the Middle Jurassic FYD quartz diorite porphyries and c.160–165 Ma Kuokeng and Tangquan adakitic rocks within the SE coastal belt have lower HREEs, but higher Ba and Sr contents, Eu/Eu*, La/Yb, Sr/Y and Gd/Yb ratios relative to the Early Jurassic Talun, JC, and Xiepu granites (Fig. 14). These indicate that the parental melts of these Middle Jurassic rocks were generated from a relatively deep source, at depths where amphibole and garnet are stable. Accordingly, the Early–Middle Jurassic granitoids along the southeast coast of China coast must have been generated in a subduction-related, compressional tectonic environment (continental arc), and Middle Jurassic crustal anatexis took place at the base of a thickened continental crust, consistent with the forward subduction of the Paleo-Pacific plate. This inference is also coincident with the geological observations that only very few Early–Middle Jurassic sedimentary sequences are distributed in southeastern China, and the Early Mesozoic sequences are generally unconformably overlain by Early Cretaceous volcaniclastic strata (He et al., 2010). The tectonic regime transition from the Tethys tectonic domain to the Pacific tectonic domain thus likely took place at ca. 200 Ma, as marked by the emplacement of the Talun I-type arc granites in southern Taiwan. Likely, the Early Jurassic magmatism along the southeast coast is genetically related to the subduction of the Paleo-Pacific plate.

6.3.2. *An integrated model for the origin of the Early–Middle Jurassic volcanic-intrusive rocks in the southeast coast of China*

It is widely recognized that granitoids formed in subduction-related environments generally have relatively high oxygen fugacity, which promotes the formation of magnetite and inhibits iron-enrichment

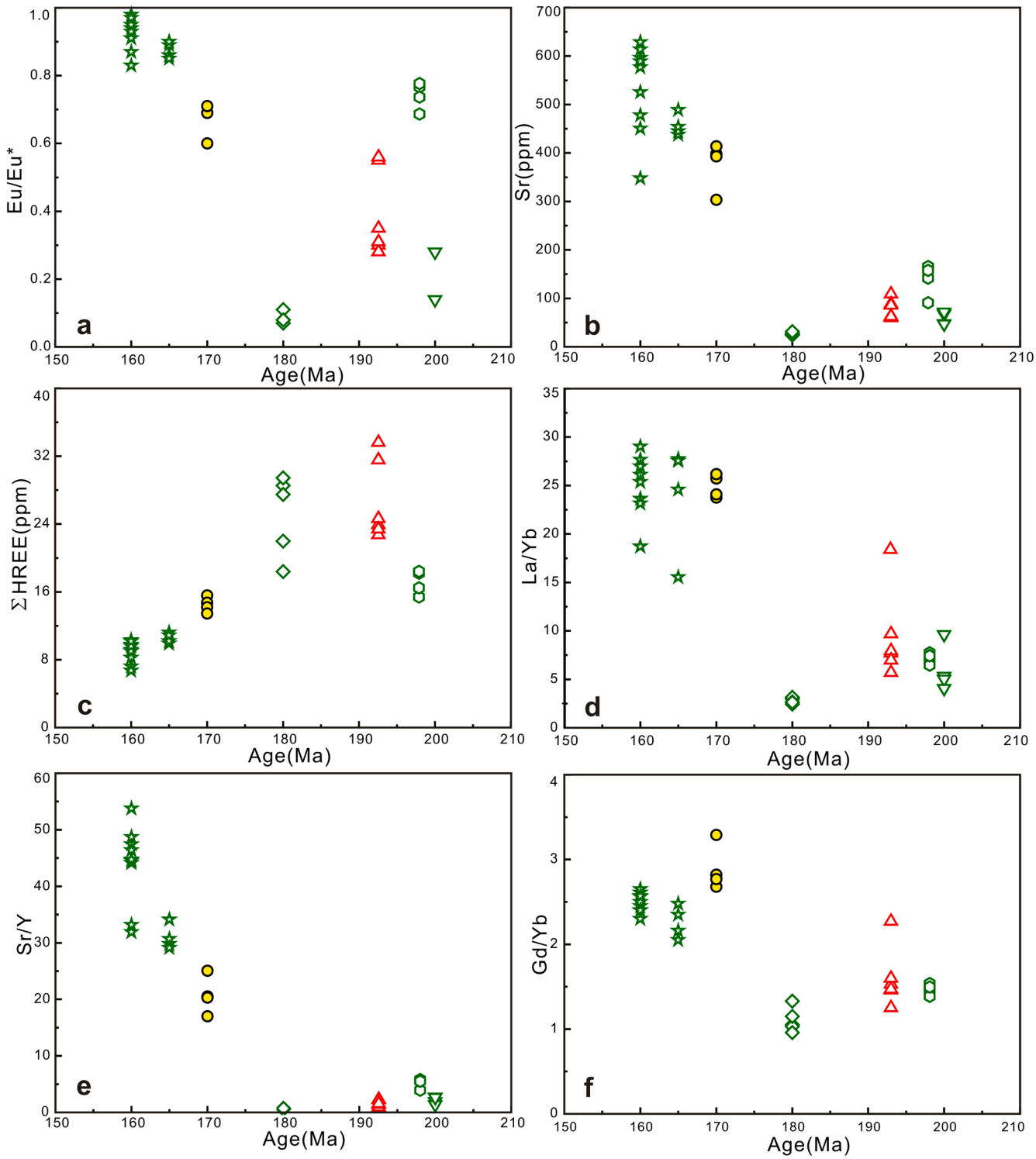

Fig. 14. Plots of Eu/Eu* (a), Sr (b), ∑HREE (c), La/Yb(d), Sr/Y(e) and Gd/Yb(f) versus ages for Early–Middle Jurassic granitoids within the coastal area of southeast China. Data sources and symbols as in Fig. 6.

during magma fractionation, and thus commonly belong to the magnesian-subtype, according to the scheme of Frost et al. (2001). In contrast, granitoids formed in extensional environments have low oxygen fugacity and are generally enriched in Fe, and therefore commonly belong to the ferroan-subtype. The $FeO^T/(FeO^T + MgO)$ ratios of the FYD quartz diorite porphyries (0.65–0.73), Early-Middle Jurassic Talun (0.70–0.81), Xiepu (0.79–0.89) and Kuokeng (0.66–0.72) granitoids and granites from the well LF3511 (0.76–0.80) within the southeast coast of China are low, typical of magnesian granitoids (Fig. 6d). By contrast, the JC granites have relatively higher $FeO^T/(FeO^T + MgO)$ values (0.82–0.87) than those of other Early–Middle Jurassic granitoids along the coast, but have similar values to the coeval A- and I-type granites within the Nanling area. This suggests that the JC granite and the coeval granitoids within the Nanling belt could be classified as ferroan granitoids (Fig. 6d). Given that vanadium is more incompatible in ferromagnesian minerals under high oxygen fugacities (Ringwood, 1955),

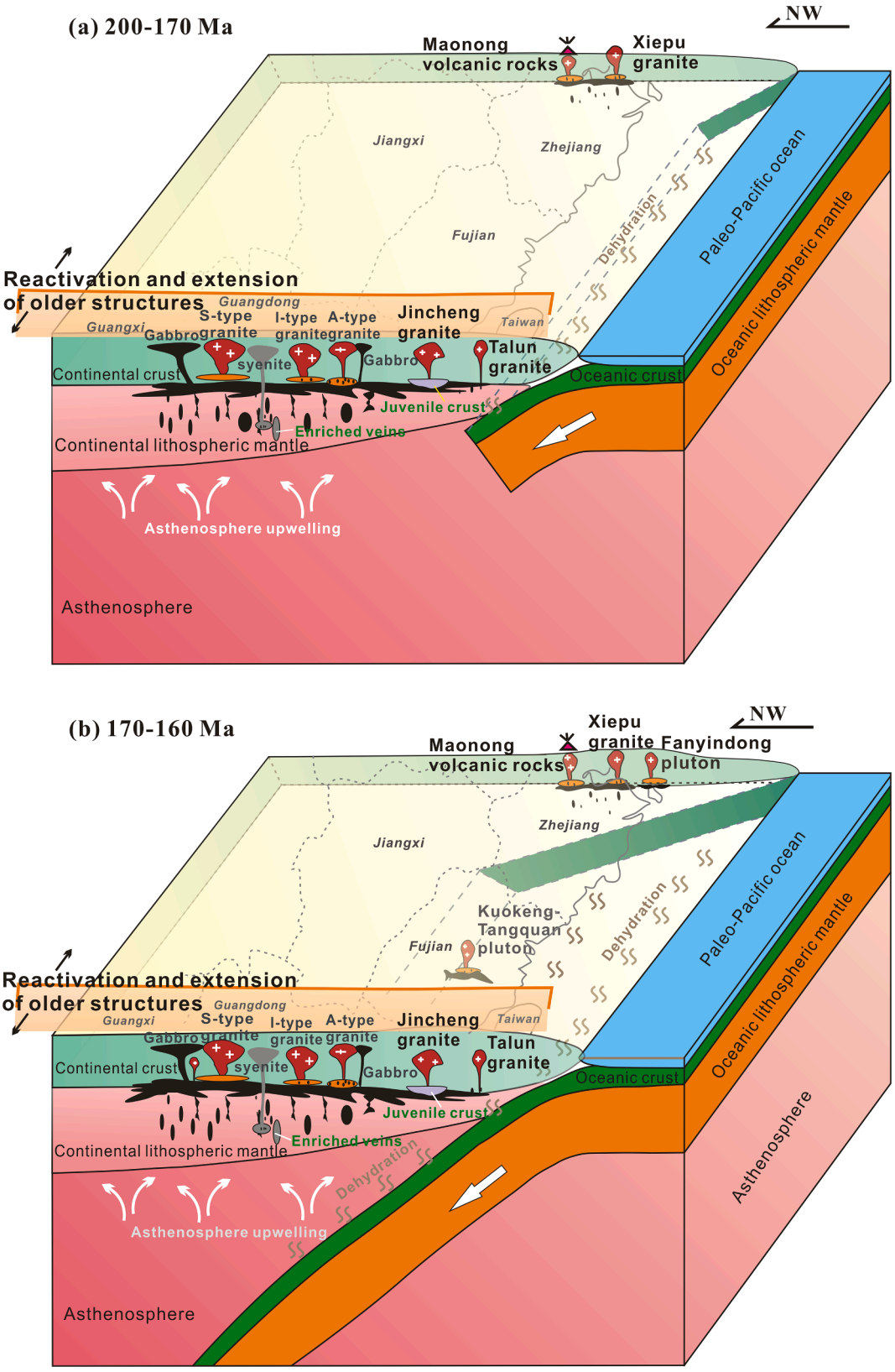

Fig. 15. Schematic representations of the Early–Middle Jurassic tectonic evolution and magmatic activities in coastal area of southeast China. (a) Northwestward subduction of the Paleo-Pacific plate beneath the South China Block during the Early Jurassic time. The subduction gave rise to the generations of the Xiepu and Maonong volcanic-intrusive rocks in southeast coast of China with arc-like geochemical affinity. At the same time, the subduction convergence stress of the Paleo-Pacific plate resulted in the reactivation of nearly E–W trending pre-existing faults, and the reactivation induced an N–S-trending, local extension in Nanling region. This extensional regime controlled the generations of the I-, A- and S-type granites, gabbro, syenite in the Nanling region and the JC granite in coastal Fujian Province. (b) Ongoing subduction of the Paleo-Pacific plate resulted in a thickening of the continental margin, and subsequent crustal anatexis of Precambrian basement materials, which produced the FYD quartz diorite porphyries and the Kuokeng-Tangquan granitoids with adakitic compositional signatures.

the concentration of V relative to other transition metals can be used as a qualitative estimate of fO_2 (Shervais, 1982). The much lower V contents and V/Sc ratios and steeper Eu–Sr slopes recorded by the ferroan JC and coeval Nanling granitoids relative to the FYD, Xiepu, and Talun magnesian granitoids indicate more reduced conditions during their generation. The JC biotite granites were emplaced within the eastern extension of the nearly E–W-striking, Nanling belt (Fig. 1). Their Sr–Nd–Hf isotopic compositions are more depleted than those of the other Early-Middle Jurassic magmatic rocks within the SE coastal belt (Figs. 8 and 9), but similar to those of coeval granitoids within the Nanling belt (Zhou et al., 2018), indicating that there was intensive crust-mantle interaction during their generation. This further supports the hypothesis that the Early–Middle Jurassic magnesian granitoids within the SE coastal belt, and the contemporaneous ferroan granites within the Nanling belt, were originally produced in different tectonic environments, and that the JC granites share a closer tectonic affinity with the coeval granites within the Nanling belt.

Yu et al. (2010) proposed that the E–W-striking magmatic belt in the Nanling region was emplaced along the boundary between the Wuyishan and the Nanling–Yunkai Precambrian terranes within the Cathaysia Block. Detailed seismic and gravity data of the Cathaysia Block indicate that there exists a WNW–ESE trending structure in the Nanling region (Zeng et al., 1997). Moreover, Jurassic granites and volcanic rocks within the Nanling belt show lower T_{DM} (<1.4 Ga) and higher $\varepsilon_{Nd}(t)$ (>−7.0) than the surrounding areas and have a nearly E–W trend (Zhou et al., 2006), overlapping with discrete gravity gradients and variations in crustal thickness in the Nanling region. Shu et al. (2004) proposed that there exists an E–W-trending ‘‘intracontinental rift belt’’, which runs from Yongding in the Fujian Province through the southern Jiangxi Province, to Shixing in the Guangdong Province (Fig. 1b), which preserves a large number of E–W trending, *syn*-sedimentary growth faults in the Early–Middle Jurassic sedimentary sequences. The development of numerous extension-related rocks in this E–W-striking magmatic belt, such as A-type granites, syenites and bimodal volcanic rock associations, as well as *syn*-sedimentary faulting strongly suggests N–S-trending extensional tectonism during the Early–Middle Jurassic in the Nanling region (He et al., 2010; Shu et al., 2004; Zhu et al., 2010). Spatial and temporal distribution of these Early–Middle Jurassic magmatic rocks indicates that an extensional tectonic regime during the Early–Middle Jurassic was largely restricted to the Nanling region, as there is only minor coeval magmatism within other parts of SE China. Zhou et al. (2018) proposed that the Jurassic magmatic rocks in the Nanling region occur along the primary faults and the basaltic rocks erupted through volcanic fissures. Taken together, this suggests that the Early–Middle Jurassic E–W-striking extension-related magmatic rocks in the Nanling belt resulted from the reactivation of pre-existing E–W striking faults due to northwestward subduction of the Paleo-Pacific plate (He et al., 2010). Both subduction of the Paleo-Pacific plate and the induced reactivation of pre-existing EW-striking faults in the Nanling region may have exerted a significant role on the petrogenesis of the JC and Talun plutons within the coastal area of southeast China.

The initiation of subduction of the Paleo-Pacific oceanic lithosphere (ca. 200 Ma) beneath the Southeast China Block not only resulted in the generation of these Early Jurassic volcanic-intrusive rocks with an arc signature along the southeast coast, such as the Talun and Maonong magmatic rocks, but also gave rise to the reactivation of a weak suture zone between the Nanling–Yunkai and Wuyishan terranes, which led to discrete and localized intraplate extension in the Nanling region (Fig. 15a). The concomitant asthenospheric mantle upwelling along this E–W-striking weak belt underwent decompression melting, which induced partial melting of the overlying metasomatized mantle. The asthenosphere-derived magmas mixed with variable amounts of magma derived from metasomatized lithospheric mantle, forming the basaltic rocks and syenites within the Nanling belt (He et al., 2010). Variable interactions between mantle- and crust-derived melts resulted in the generation of the S-, I- and A-type granites in the Nanling belt (Fig. 15a, He et al., 2010; Zhu et al., 2010). At the same time, mantle-derived magma underplated pre-existing lower crust to form the juvenile crust in the eastern section of the E–W-striking Nanling magmatic belt, under the combined action of the subduction of the Paleo-Pacific plate and the induced local intraplate extension. Partial melting of the juvenile crust materials produced the Tiandong granite in the northeastern Guangdong province (188 Ma, Zhou et al., 2018) and the JC granite in the coastal Fujian Province (Fig. 15a), with significantly depleted isotopic signatures. Subsequently, ongoing subduction of the Paleo-Pacific plate resulted in continental crust thickening along the coast of southeast China at c. 170 Ma, and partial melting of this thickened lower crust formed the FYD and Kuokeng-Tangquan plutons in SE China coast with minor to no involvement of mantle-derived magmas (Fig. 15b, Li et al., 2016a; Wang et al., 2015).

7. Conclusions

(1) The FYD quartz diorite porphyry and JC biotite granite from the southeast coast of China were emplaced at 170 Ma and 193 Ma, respectively. Data from this study, combined with previous geochronological and geochemical data, determine a NE-trending, Early–Middle Jurassic, arc-related magmatic rock belt along the southeast coast of China.

(2) This study offers the most enriched Sr–Nd–Hf isotopic compositions to ever be reported for the Mesozoic granitioids within southeast China, suggesting that ancient basement rocks similar to the Badu complex also are distributed under the deep crust of the southeast coast of China. Underplating of mantle-derived mafic magma, especially during the Mesozoic, resulted in gradual modification and vertical growth of the pre-existing lower crust beneath the coastal area of southeast China.

(3) Both new and previous data suggest that the Paleo-Pacific plate subduction underneath southeast China most likely started at ca. 200 Ma. The generation of the JC granites was controlled by the subduction of the Paleo-Pacific plate and the induced reactivation of pre-existing E-W-striking faults in the Nanling region. Ongoing subduction of the Paleo-Pacific plate resulted in the thickening of the continental margin. Subsequent crustal anatexis produced the FYD quartz diorite porphyries with adakitic compositional signatures.

CRediT authorship contribution statement

Jiao-Long Zhao: Investigation, Conceptualization, Methodology, Software, Data curation, Formal analysis, Writing - original draft, Writing - review & editing, Project administration, Funding acquisition. **Jian-Sheng Qiu:** Investigation, Conceptualization, Formal analysis, Writing - original draft, Project administration, Funding acquisition. **Liang Liu:** Investigation, Conceptualization, Writing - review & editing.

Declaration of Competing Interest

The authors declare that they have no known competing financial interests or personal relationships that could have appeared to influence the work reported in this paper.

Acknowledgements

This study was financially supported by the National Key R&D Program of China (2016YFC0600405) and National Natural Science Foundation of China (Grant nos. 41702048 and 41872052).

References

Altherr, R., Holl, A., Hegner, E., Langer, C., Kreuzer, H., 2000. High-potassium, calc-alkaline I-type plutonism in the European Variscides: northern Vosges (France) and northern Schwarzwald (Germany). Lithos 50, 51–73.

Andersen, T., 2002. Correction of common lead in U-Pb analyses that do not report 204Pb. Chem. Geol. 192, 59–79.

Bai, Z.J., Zhu, W.G., Zhong, H., Li, C.S., Liao, J.Q., Sun, H.S., 2015. Petrogenesis and tectonic implications of the early Jurassic Fe–Ti oxide-bearing Xialan mafic intrusion in SE China: Constraints from zircon Hf–O isotopes, mineral compositions and whole-rock geochemistry. Lithos 212–215, 59–73.

Black, L.P., Gulson, B.L., 1978. The age of the mud tank carbonatite, Strangways range, Northern territory. BMR J. Australian Geol. Geophys. 3, 227–232.

Blichert-Toft, J., Albarède, F., 1997. The Lu-Hf geochemistry of chondrites and evolution of the mantle-crust system. Earth Plan. Sci. Lett. 148 (1–2), 243–258.

Boynton, W.V., 1984. Geochemistry of the rare earth elements: meteorite studies. In: Henderson, P. (Ed.), Rare Earth Elements Geochemistry. Elservier, Amsterdam, pp. 63–144.

Cen, T., Li, W.X., Wang, X.C., Pang, C.J., Li, Z.X., Xing, G.F., Zhao, X.L., Tao, J.H., 2016. Petrogenesis of early Jurassic basalts in southern Jiangxi Province, South China: Implications for the thermal state of the Mesozoic mantle beneath South China. Lithos 256–257, 311–330.

Chappell, B.W., White, A.J.R., 1974. Two contrasting granite types. Pac. Geol. 8, 173–174.

Chen, B., Jahn, B.M., Suzuki, K., 2013a. Petrological and Nd-Sr-Os isotopic constraints on the origin of high-Mg adakitic rocks from the North China Craton: tectonic implications. Geology 41, 91–94.

Chen, C.H., Lee, C.Y., Shinjo, R., 2008. Was there Jurassic paleo-Pacific subduction in South China?: constraints from $^{40}Ar/^{39}Ar$ dating, elemental and Sr-Nd-Pb isotopic geochemistry of the Mesozoic basalts. Lithos 106 (1–2), 83–92.

Chen, J.F., Jahn, B., 1998. Crustal evolution of southeastern China: Nd and Sr isotopic evidence. Tectonophysics 284, 101–133.

Chen, J.Y., Yang, J.H., Ji, W.Q., 2017. Ages and petrogenesis of Jurassic and cretaceous intrusive rocks in the Matsu Islands: Implications for lower crust modification beneath southeastern China. J. Asian Earth Sci. 150, 14–24.

Chen, J.Y., Yang, J.H., Zhang, J.H., Sun, J.F., Wilde, S.A., 2013b. Petrogenesis of the Cretaceous Zhangzhou batholith in southeastern China: zircon U-Pb age and Sr-Nd-Hf-O isotopic evidence. Lithos 162–163, 140–156.

Chen, P.R., Hua, R.M., Tong, Z.B., Lu, J., Fan, C., 2002. Early Yanshanian post-orogenic granitoids in the Nanling region: petrological constraints and geodynamic settings. Sci. China (Series D) 45 (8), 755–768.

Chen, R., Xing, G.F., Yang, Z.L., Zhou, Y.Z., Yu, M.G., Li, L.M., 2005. The geochemical characteristics and geological implication of the early Mesozoic volcanic-intrusive rocks in eastern Zhejiang Province. The fourth national symposium on volcanoes, Beihai, China, pp. 5–6.

Davies, J.H., von Blanckenburg, F., 1995. Slab breakoff: a model of lithosphere detachment and its test in the magmatism and deformation of collisional orogens. Earth Planet. Sci. Lett. 129, 85–102.

Defant, M.J., Drummond, M.S., 1990. Derivation of some modern arc magmas by melting of young subducted lithosphere. Nature 347, 662–665.

Frost, B.R., Barnes, C.G., Collins, W.J., Arculus, R.J., Ellis, D.J., Frost, C.D., 2001. A geochemical classification for granitic rocks. J. Petrol. 42, 2033–2048.

Gao, J.F., Lu, J.J., Lin, Y.P., Pu, W., 2003. Analysis of trace elements in rock samples using HR-ICPMS. J. Nanjing Univ. (Nat. Sci.) 39, 844–850 (in Chinese with English abstract).

Ge, X.Y., Li, X.H., Chen, Z.G., Li, W.P., 2002. Geochemistry and petrogenesis of Jurassic high Sr/low Y granitoids in eastern China: constrains on crustal thickness. Chin. Sci. Bull. 47 (11), 962–968.

Griffin, W.L., Pearson, N.J., Belousova, E.A., 2007. Reply to "Comment to short-communication 'Comment: Hf –isotope heterogeneity in zircon 91500' by W.L. Griffin, N.J. Pearson, E.A. Belousova and A. Saeed (Chemical geology 233 (2006) 358-363)" by F. Corfu. Chem. Geol. 244(1–2), 354–356.

He, Z.Y., Xu, X.S., Niu, Y.L., 2010. Petrogenesis and tectonic significance of a Mesozoic granite-syenite-gabbro association from inland South China. Lithos 119 (3–4), 621–641.

Irvine, T.N., Baragar, W.R.A., 1971. A guide to the chemical classification of the common volcanic rocks. Can. J. Earth Sci. 8, 523–548.

Jackson, S.E., Pearson, N.J., Griffin, W.L., Belousoval, E.A., 2004. The application of laser ablation-inductively coupled plasma-mass spectrometry (LA-ICP-MS) to in situ U-Pb zircon geochronology. Chem. Geol. 211, 47–69.

Jiang, Y.H., Wang, G.C., Liu, Z., Ni, C.Y., Qing, L., Zhang, Q., 2015. Repeated slab-advance-retreat of the Palaeo-Pacific plate underneath SE China. Int. Geol. Rev. 57, 472–491.

Jiang, Y.H., Wang, G.C., Qing, L., Zhu, S.Q., Ni, C.Y., 2017. Early Jurassic A-type granites in SE China: shallow dehydration melting of early Paleozoic granitoids by basaltic magma intraplating. J. Geol. 125, 351–366.

Kemp, A.I.S., Wormald, R.J., Whitehouse, M.J., Price, R.C., 2005. Hf isotopes in zircon reveal contrasting sources and crystallization histories for alkaline toperalkaline granites of Temora, southeastern Australia. Geology 33 (10), 797–800.

Li, B., Jiang, S.Y., Zhang, Q., Zhao, H.X., Zhao, K.D., 2016a. Geochemistry, geochronology and Sr–Nd–Pb–Hf isotopic compositions of Middle to Late Jurassic syenite–granodiorites–dacite in South China: Petrogenesis and tectonic implications. Gondwana Res. 35, 217–237.

Li, S.N., Ni, P., Wang, G.G., Bao, T., Huang, B., Dai, B.Z., 2020. The Jurassic volcanic–intrusive complex in the Dehua gold orefield, coastal region of SE China: Implications for the tectonic setting and epithermal mineralization. J. Asian Earth Sci. 197, 104390.

Li, W.Y., Ma, C.Q., Liu, Y.Y., Robinson, P.T., 2012a. Discovery of the Indosinian aluminum A-type granite in Zhejiang Province and its geological significance. Sci. China (Earth Sciences) 1, 16–28.

Li, X.H., Chung, S.L., Zhou, H., Lo, C.H., Liu, Y., Chen, C.H., 2004. Jurassic intraplate magmatism in southern Hunan-eastern Guangxi: 40Ar/39Ar dating, geochemistry, Sr-Nd isotopes and implications for the tectonic evolution of SE China. Geol. Soc. London, Special Publication 226 (1), 193–215.

Li, X.H., Li, W., Li, Z., Lo, C., Wang, J., Ye, M., Yang, Y., 2009. Amalgamation between the Yangtze and Cathaysia Blocks in South China: Constraints from SHRIMP U-Pb zircon ages, geochemistry and Nd-Hf isotopes of the Shuangxiwu volcanic rocks. Precambrian Res. 174, 117–128.

Li, X.H., Li, Z.X., Li, W.X., 2014a. Detrital zircon U-Pb age and Hf isotope constrains on the generation and reworking of Precambrian continental crust in the Cathaysia Block, SouthChina: A synthesis. Gondwana Res. 25, 1202–1215.

Li, Y.J., Wei, J.H., Santosh, M., Tan, J., Fu, L.B., Zhao, S.Q., 2016b. Geochronology and petrogenesis of Middle Permian S-type granitoid in southeastern Guangxi Province, South China: Implications for closure of the eastern Paleo-Tethys. Tectonophysics 682, 1–16.

Li, Z., Qiu, J.S., Xu, X.S., 2012b. Geochronological, geochemical and Sr-Nd-Hf isotopic constraints on petrogenesis of Late Mesozoic gabbro-granite complexes on the southeast coast of Fujian, South China: insights into a depleted mantle source region and crustmantle interactions. Geol. Mag. 149 (3), 459–482.

Li, Z., Qiu, J.S., Yang, X.M., 2014b. A review of the geochronology and geochemistry of Late Yanshanian (Cretaceous) plutons along the Fujian coastal area of southeastern China: Implications for magma evolution related to slab break-off and rollback in the Cretaceous. Earth Sci. Rev. 128, 232–248.

Li, Z.X., Li, X.H., 2007. Formation of the 1300-km-wide intracontinental orogen and postorogenic magmatic province in Mesozoic South China: a flat-slab subduction model. Geology 35 (2), 179–182.

Li, Z.X., Li, X.H., Chung, S.L., Lo, C.H., Xu, X.S., Li, W.X., 2012c. Magmatic switch-on and switch-off along the South China continental margin since the Permian: transition from an Andean-type to a Western Pacific-type plate boundary. Tectonophysics 532–535, 271–290.

Liu, J.X., Wang, S., Wang, X.L., Du, D.H., Xing, G.F., Fu, J.M., Chen, X., Sun, Z.M., 2020. Refining the spatio-temporal distributions of Mesozoic granitoids and volcanic rocks in SE China. J. Asian Earth Sci. https://doi.org/10.1016/j.jseaes.2020.104503.

Liu, L., Qiu, J.S., Li, Z., 2013. Origin of mafic microgranular enclaves (MMEs) and their host quartz monzonites from the Muchen pluton in Zhejiang Province, Southeast China: implications for magma mixing and crust–mantle interaction. Lithos 160–161, 145–163.

Liu, L., Xu, X.S., Zou, H.B., 2012. Episodic eruptions of the late Mesozoic volcanic sequences in southeastern Zhejiang, SE China: petrogenesis and implications for the geodynamics of paleo-Pacific subduction. Lithos 154, 166–180.

Liu, Q., Yu, J.H., O'Reilly, S.Y., Zhou, M.F., Griffin, W.L., Wang, L.J., Cui, X., 2014. Origin and geological significance of Paleoproterozoic granites in the northeastern Cathaysia Block, South China. Precambr. Res. 248, 72–95.

Liu, Q., Yu, J.H., Su, B., Wang, Q., Tang, H.F., Xu, H., Cui, X., 2011. Discovery of the 187Ma granite in Jincheng area, Fujian Province: constraint on Early Jurassic tectonic evolution of southeastern China. Acta PetrologicaSinica 27 (12), 3575–3589 (in Chinese with English abstract).

Maniar, P.D., Piccoli, P.M., 1989. Tectonic discrimination of granitoids. Geol. Soc. Am. Bull. 101, 635–643.

McDonough, W.F., Sun, S.S., 1995. The composition of the Earth. Chem. Geol. 120, 223–253.

Middlemost, E.A.K., 1994. Naming materials in the magma/igneous rock system. Earth-Sci. Rev. 37, 215–224.

Miller, R.G., O'Nions, R.K., 1985. Source of Precambrian chemical and clastic sediments. Nature 314, 325–330.

Niu, Y.L., Zhao, Z.D., Zhu, D., Mo, X.X., 2013. Continental collision zones are primary sites for net continental crust growth — A testable hypothesis. Earth Sci. Rev. 127, 96–110.

PatiñoDouce, A.E., 1999. What do experiments tell us about the relative contributions of crust and mantle to the origin of granitic magmas? In: Castro, A., Fernandez, C., Vjgneress, J.L. (Eds.), Understanding Granites: Integrating New and Classical Techniques. Spec. Public Geol. Soc. London 168, pp. 55–75.

Pearce, J.A., Harris, N.B.W., Tindle, A.G., 1984. Trace element discrimination diagrams for the tectonic interpretation of granitic rocks. J. Petrol. 25, 956–983.

Peccerillo, A., Taylor, D.R., 1976. Geochemistry of Eocene calc-alkaline volcanic rocks from the Kaitamonu area, Northern Turkey. Contrib. Miner. Petrol. 58, 63–91.

Pu, W., Gao, J.F., Zhao, K.D., Lin, H.F., Jiang, S.Y., 2005. Separation method of Rb-Sr, Sm-Nd using DCTA and HIBA. J. Nanjing Univ. (Nature Sciences) 41, 445–450 (in Chinese with English abstract).

Qian, Q., Hermann, Jörg, 2013. Partial melting of lower crust at 10–15 kbar: constraints on adakite and TTG formation. Contrib. Miner. Petrol. 165, 195–1224.

Qiu, J.S., Li, Z., Liu, L., Zhao, J.L., 2012. Petrogenesis of the Zhangpu composite granite pluton in Fujian Province: constraints from zircon U-Pb ages, elements geochemistry and Nd-Hf isotopes. Acta Geol. Sin. 86 (4), 561–576 (in Chinese with English abstract).

Richards, J.P., Spell, T., Rameh, E., Razique, A., Fletcher, T., 2012. High Sr/Y magmas reflect arc maturity, high magmatic water content, and porphyry Cu ± Mo ± Au potential: examples from the Tethyan arcs of central and eastern Iran and western Pakistan. Econ. Geol. 107, 295–332.

Ringwood, A.E., 1955. The principles governing trace-element behaviour during magmatic crystallization: part II. The role of complex formation. Geochimica et CosmochimicaActa 7, 242–254.
Shervais, J.W., 1982. Ti–V plots and the petrogenesis of modern and ophiolitic lavas. Earth Planet. Sci. Lett. 59, 101–118.
Shu, L.S., Faure, M., Yu, J.H., Jahn, B.M., 2011. Geochronological and geochemical features of the Cathaysia block (South China): New evidence for the Neoproterozoic breakup of Rodinia. Precambr. Res. 187, 263–276.
Shu, L.S., Zhou, X.M., Deng, P., Yu, X.Q., Wang, B., Zu, F.P., 2004. Geological features and tectonic evolution of Meo-Cenozoic basins in southeastern China. Geological Bulletin of China 23, 876–884.
Sisson, T., Ratajeski, K., Hankins, W., Glazner, A., 2005. Voluminous granitic magmas from common basaltic sources. Contrib. Miner. Petrol. 148, 635–661.
Soderlund, U., Patchett, P.J., Vervoort, J.D., Isachsen, C.E., 2004. The ^{176}Lu decay constant determined by Lu-Hf and U-Pb isotope systematics of Precambrian mafic intrusions. Earth Planet. Sci. Lett. 219, 311–324.
Wang, G.C., Jiang, Y.H., Liu, Z., Ni, C.Y., Qing, L., Zhang, Q., 2015. Elemental and Sr-Nd-Hf isotopic constraints on the origin of Late Jurassic adakitic granodiorite in central Fujian province, southeast China. Mineral. Petrol. 109, 501–518.
Wang, Q., Li, J.W., Jian, P., Zhao, Z.H., Xiong, X.L., Bao, Z.W., Xu, J.F., Li, C.F., Ma, J.L., 2005. Alkaline syenites in eastern Cathaysia (South China): link to Permian-Triassic transtension. Earth Planet. Sci. Lett. 230, 339–354.
Wang, X., Zhou, J.C., Qiu, J.S., Zhang, G.L., 2006. LA-ICP-MS U-Pb zircon geochronology of the Neoproterozoic igneous rocks from Northern Guangxi, South China: implications for tectonic evolution. Precambr. Res. 145 (1–2), 111–130.
Vervoort, J.D., Blichert-Toft, J., 1999. Evolution of the depleted mantle: Hf isotope evidence from juvenile rocks through time. Geochim. Cosmochim. Acta 63, 533–556.
Wang, Y.J., Gan, C.S., Tan, Q.L., Zhang, Y.Z., He, H.Y., Xin, Q., Zhang, Y.H., 2018. Early Neoproterozoic (~840 Ma) slab window in South China: Key magmatic records in the Chencai Complex. Precambr. Res. 314, 434–451.
Wang, G.G., Ni, Pei, Zhao, Kui-Dong, Wang, Xiao-Lei, Liu, Ji-Qiang, Jiang, Shao-Yong, Chen, Hui, 2012. Petrogenesis of the Middle Jurassic Yinshan volcanic-intrusive complex, SE China: implications for tectonic evolution and Cu-Au mineralization. Lithos 150, 135–154.
Wang, Z.Y., Zhao, X.L., Yu, S.Y., Li, S.Z., Peng, Y.B., Liu, Y.J., 2020. Cretaceous granitic intrusions in Fujian Province, Cathaysia Block: Implications for slab rollback and break-off of the Paleo-Pacific plate. J. Asian Earth Sci. 190, 104164.
Williams, I., Buick, I., Cartwright, I., 1996. An extended episode of early Mesoproterozoic metamorphic fluid flow in the Reynolds Range, central Australia. J. Metamorph. Geol. 14, 29–47.
Wong, J., Sun, M., Xing, G., Li, X., Zhao, G., Wong, K., Yuan, C., Xia, X., Li, L., Wu, F., 2009. Geochemical and zircon U-Pb and Hf isotopic study of the Baijuhuajian metaluminous A-type granite: extension at 125–100 Ma and its tectonic significance for South China. Lithos 112, 289–305.
Wu, F.Y., Jahn, B.M., Wilde, S., Sun, D.Y., 2000. Phanerozoic crustal growth: U-Pb and Sr–Nd isotopic evidence from the granites in northeastern China. Tectonophysics 328, 89–113.
Wu, F.Y., Jahn, B.M., Wilde, S.A., Lo, C.H., Yui, T.F., Lin, Q., Ge, W.C., Sun, D.Y., 2003. Highly fractionated I-type granites in NE China (II): Isotopic geochemistry and implications for crustal growth in the Phanerozoic. Lithos 67, 191–204.
Xia, Y., Xu, X.S., Zhu, K.Y., 2012. Paleoproterozoic S- and A-type granites in southwestern Zhejiang: magmatism, metamorphism and implications for the crustal evolution of the Cathaysia basement. Precambrian Res. 216–219, 177–207.
Xu, X.S., O'Reilly, S.Y., Griffin, W.L., Pearson, N.J., He, Z.Y., 2007. The crust of Cathaysia: age, assembly and reworking of two terranes. Precambr. Res. 158, 51–78.
Xu, C., Zhang, L., Shi, H.S., Brix, M.R., Huhma, H., Chen, L.H., Zhang, M.Q., Zhou, Z.Y., 2017. Tracing an Early Jurassicmagmatic arc from South to East ChinaSeas. Tectonics 36, 466–492.
Yang, J.B., Zhao, Z.D., Hou, Q.Y., Niu, Y.L., Mo, X.X., Sheng, D., Wang, L.L., 2018. Petrogenesis of Cretaceous (133–84 Ma) intermediate dykes and host granites in southeastern China: Implications for lithospheric extension, continental crustal growth, and geodynamics of Palaeo-Pacific subduction. Lithos 296–299, 195–211.
Yang, Y., Zhang, H., Chu, Z., Xie, L., Wu, F., 2010. Combined chemical separation of Lu, Hf, Rb, Sr, Sm and Nd from a single rock digest and precise and accurate isotope determinations of Lu–Hf, Rb–Sr and Sm–Nd isotope systems using Multi-Collector ICP-MS and TIMS. Int. J. Mass Spectrom 290, 120–126.
Yu, J.H., O'Reilly, S.Y., Zhou, M.F., Griffin, W.L., Wang, L.J., 2012. U-Pb geochronology and Hf–Nd isotopic geochemistry of the Badu Complex, Southeastern China: implications for the Precambrian crustal evolution and paleogeography of the Cathaysia Block. Precambr. Res. 222–223, 424–449.
Yu, J.H., O'Reilly, S.Y., Suzanne, Y., Wang, L.J., Griffin, W.L., Zhou, M.F., Zhang, M., Shu, L.S., 2010. Components and episodic growth of Precambrian crust in the Cathaysia Block, South China: Evidence from U-Pb ages and Hf isotopes of zircons in Neoproterozoic sediments. Precambr. Res. 181 (1–4), 97–114.
Yui, T.F., Chu, H.T., Suga, K., Lan, C.Y., Chung, S.H., Wang, K.L., Grove, M., 2017. Subduction-related 200 Ma Talunmetagranite, SE Taiwan: an age constraint for palaeo-Pacific plate subduction beneath South China Block during the Mesozoic. Int. Geol. Rev. 59 (3), 333–346.
Zeng, H., Zhang, Q., Li, Y., Liu, J., 1997. Crustal structure inferred from gravity anomalies in South China. Tectonophysics 283, 189–203.
Zhao, J.L., Qiu, J.S., Liu, L., Wang, R.Q., 2016. The late cretaceous I- and A-type granite association of Southeast China: Implications for the origin and evolution of postcollisional extensional magmatism. Lithos 240–243, 16–33.
Zhao, Z.F., Gao, P., Zheng, Y.F., 2015. The source of Mesozoic granitoids in South China: Integrated geochemicalconstraints from the Taoshan batholith in the Nanling Range. Chem. Geol. 395, 11–26.
Zheng, Y.F., Zhang, S.B., Zhao, Z.F., Wu, Y.B., Li, X., Li, Z., Wu, F.Y., 2007. Contrasting zircon Hf and O isotopes in the two episodes of Neoproterozoic granitoids in South China: Implications for growth and reworking of continental crust. Lithos 96 (1–2), 127–150.
Zheng, Y.F., Wu, R.X., Wu, Y.B., Zhang, S.B., Yuan, H., Wu, F.-Y., 2008. Rift melting of juvenile arc-derived crust: Geochemical evidence from Neoproterozoic volcanic and granitic rocks in the Jiangnan Orogen, South China. Precambr. Res. 163 (3–4), 351–383.
Zhou, X.M., Sun, T., Shen, W.Z., Shu, L.S., Niu, Y.L., 2006. Petrogenesis of Mesozoic granitoids and volcanic rocks in South China: a response to tectonic evolution. Episodes 29, 26–33.
Zhou, Z.M., Ma, C.Q., Wang, L.X., Chen, S.G., Xie, C.F., Li, Y., Liu, W., 2018. A source-depleted Early Jurassic granitic pluton from South China: Implication to the Mesozoic juvenile accretion of the South China crust. Lithos 300–301, 278–290.
Zhu, K.Y., Li, Z.X., Xu, X.S., Wilde, S.A., 2013. Late Triassic melting of a thickened crust in southeastern China: evidence for flat-slab subduction of the Paleo-Pacific plate. J. Asian Earth Sci. 74, 265–279.
Zhu, W.G., Zhong, H., Li, X.H., He, D.F., Song, X.Y., Ren, T., Chen, Z.Q., Sun, H.S., Liao, J. Q., 2010. The early Jurassic mafic–ultramafic intrusion and A-type granite from northeastern Guangdong, SE China: age, origin, and tectonic significance. Lithos 119, 313–329.